J Sci Comput (2012) 52:675–703
DOI 10.1007/s10915-011-9566-3

Influence of Reference-to-Physical Frame Mappings on Approximation Properties of Discontinuous Piecewise Polynomial Spaces

Lorenzo Botti

Received: 9 April 2011 / Revised: 9 September 2011 / Accepted: 28 November 2011 /
Published online: 17 December 2011

Abstract In this manuscript we compare physical and reference frame discontinuous Galerkin (dG) discretizations with emphasis on the influence of reference-to-physical frame mappings on the discrete space properties. We assess the excellence of physical frame discrete spaces in terms of approximation capabilities as well as the increased flexibility compared to reference frame discretizations. As a matter of fact, whenever curved elements are considered, non-affine reference-to-physical frame mappings are able to spoil the convergence properties of reference frame discrete spaces. This poorly documented drawback does not affect basis functions defined directly in the physical frame.

The convergence degradation associated to reference frame discretizations is evaluated theoretically, providing error bounds for the approximation error of the L^2-orthogonal projection operator, and the findings are justified by means of numerical test cases. In particular we exemplify by means of quadrilateral elements grids challenging grid configurations characterized by non-affine mappings and demonstrate the ability to predict the convergence rates without stringent assumptions on the element shapes.

Keywords Discontinuous Galerkin methods · Physical frame discretization · Reference-to-physical frame mapping · Quadrilateral elements · Convergence degradation

1 Introduction

In this work we investigate the approximation properties of reference and physical frame piecewise polynomial discrete spaces in the context of discontinuous Galerkin (dG) methods.

L. Botti (✉)
Dipartimento di Ingegneria Industriale, Università degli Studi Di Bergamo, Via Marconi 5,
24044 Dalmine, BG, Italy
e-mail: lorenzo.botti@unibg.it

L. Botti
Biomedical Engineering Department, Mario Negri Institute for Pharmacological Research, Ranica, Italy

Let Ω be a bounded connected open domain, and let $\mathcal{T}_h$ denote a general mesh of Ω composed of elements with possibly curved edges. The introduction of an auxiliary, reference frame set of standardized polygons is a common practice as it allows to define discrete approximation spaces as a combination of a mesh independent function and a geometric transformation inherited from the mesh topology, see e.g. Ern and Guermond [8]. The geometric transformation is specific to each element of the computational mesh, and, since it allows to map the reference frame polygon onto the physical frame mesh element, it is hereafter referred to as *reference-to-physical frame mapping function*.

In continuous Galerkin (cG) discretizations, the introduction of a reference frame basis function definition makes it straightforward to impose the continuity at element interfaces allowing to easily deal with hybrid two- and three-dimensional meshes. In dG methods the inter-element continuity is not required leading to an increased flexibility in the definition of discrete polynomial spaces. Even if reference frame basis functions are still the preferred choice for dG practitioners, an interesting and little-known point is that physical frame discretizations lead to optimal order of approximation on general meshes while reference frame discretizations might suffer from a convergence degradation issue closely related to the shape of the mesh elements and the discrete approximation space properties.

Error estimates in the context of non-affine finite elements has been proved since the early efforts of Ciarlet and Raviart [6] and the case of anisotropic meshes has recently received attention, see e.g. Georgoulis [10]. Accuracy deteriorations have been acknowledged by several authors who adopted reference frame discretizations of boundary values problems with stiff constraints on the domain geometry, e.g. Kurtz and Xenophontos [13], in the Reissner-Mindlin plate problem, and Suri [16], where the phenomenon of *numerical locking* in thin domains is investigated. MacNeal and Harder [14] and later Kikuchi, Okabe and Fujio [12] noticed the different performance of eight- and nine-node quadrilaterals and proposed a modification of the eight-node serendipity element with better interpolation properties, see also Zhang and Kikuchi [19]. Recently, a paper of Arnold, Boffi and Falk [2] has investigated theoretically and numerically the convergence degradation of reference frame discretization on general quadrilateral meshes with straight edges. This latter work has been of great inspiration for the realization of this manuscripts.

In this paper we provide error bounds for the approximation error of the L^2-orthogonal projection operator on general meshes and we characterize what is needed for optimal order approximation in the context of reference frame discretizations. Thanks to the version of the Bramble-Hilbert lemma introduced by Brenner and Scott [5] we first prove optimal order of approximation for physical frame discretizations on general meshes. As a second step we investigate the effects of non-linear reference-to-physical frame mappings on reference frame discretizations. Inspired by the work of Arnold, Boffi and Falk, we ought to demonstrate that it is possible to build a reference frame polynomial space that is a supersets of a physical frame polynomial space, or, similarly, to identify a physical frame polynomial space as a subset of a reference frame polynomial space. Moreover, we further exploit this possibility to accurately estimate the convergence rates associated to reference frame discretization by means of the theoretical results here obtained in the context of physical frame discretizations.

The influence of geometric transformations is numerically assessed on regular mesh sequences featuring non-affine reference-to-physical frame mappings, in particular we consider square grids, distorted quadrilateral meshes and quadrilateral meshes with curved edges. We compare physical and reference frame discretizations evaluating the p-refinement accuracy and we demonstrate the ability to predict the theoretical h-convergence rates. Although developed and tested in the context of quadrilateral elements meshes, the theory here

presented can be easily extended to triangles and three dimensional cells like hexahedrals, prisms and tetrahedrals admitting a reference frame analogue.

The material is organized as follows. In Sect. 2 we introduce physical and reference frame discrete polynomial spaces and briefly describe the main ingredients required to build a finite element discretization, that is basis functions and mapping functions. Section 3 is devoted to approximation capabilities of discrete spaces and contains the main results of this work. We demonstrate optimal approximation properties for physical frame dG approximation on regular mesh sequences, see Sect. 3.1, and investigate the convergence degradation associated to reference frame discretization when general meshes are considered, refer to Sect. 3.2. In Sect. 4, after a brief discussion on numerical integration issues, we perform a series of test cases to numerically assess the theoretical estimates on the convergence rates. Firstly we focus on the L^2-orthogonal projection underling the differences between reference and physical frame approximations, see Sect. 4.2. Finally, in Sect. 4.3, we tackle the Interior Penalty dG discretization of the Laplace equation on general meshes.

2 Reference and Physical Space Basis Functions

2.1 Physical Frame Basis Functions

Physical frame dG discretizations has been considered by several authors, e.g. Gassner, Lörcher, Munz and Hesthaven [9], Bassi, Crivellini, Di Pietro and Rebay [4], and proposed as a key instrument to build dG approximations with optimal approximation properties, see Di Pietro and Ern [7, Chap. 1].

Let $\Omega \subset \mathbb{R}^d$, $d = 2$ and consider a mesh $\mathcal{T}_h$ composed of quadrilateral elements $E \in \mathcal{T}_h$ with possibly curved edges. We consider the spaces

$$\mathbb{P}^k(\mathcal{T}_h) \stackrel{\text{def}}{=} \left\{ v_h \in L^2(\Omega) \mid v_{h|E} \in \mathbb{P}^k(E), \forall E \in \mathcal{T}_h \right\}, \tag{1}$$

where k is a non-negative integer and $\mathbb{P}^k(E)$ denotes the restriction to a mesh element E of the polynomial functions of two variables and total degree $\leq k$, so that $\dim(\mathbb{P}^k) = \frac{(k+1)(k+2)}{2}$.

For all $E \in \mathcal{T}_h$, we denote by $N_{\text{dof}}^{\mathbb{P}^k}$ the dimension of the local polynomial space $\mathbb{P}^k(E)$ and set $D_{\mathbb{P}^k} \stackrel{\text{def}}{=} \{1, \ldots, N_{\text{dof}}^{\mathbb{P}^k}\}$. For a given $E \in \mathcal{T}_h$, let $\Phi^k_{\mathbb{P}(E)} = \{\varphi_i^E\}_{i \in D_{\mathbb{P}^k}}$ denote a basis for $\mathbb{P}^k(E)$. The functions φ_i^E, $i \in D_{\mathbb{P}^k}$, can be extended to Ω by simply setting $\varphi_i^E = 0$ on $\Omega \setminus E$. A basis for the space $\mathbb{P}^k(\mathcal{T}_h)$ is then given by

$$\Phi^k \stackrel{\text{def}}{=} \{\Phi^k_{\mathbb{P}(E)}\}_{E \in \mathcal{T}_h}. \tag{2}$$

By construction, the support of each basis function in Φ^k is contained in exactly one element.

Physical space basis functions are defined so to inherently span the space $\mathbb{P}^k(\mathcal{T}_h)$ even in case of arbitrarily shaped elements with possibly curved edges. From a practical viewpoint, in order to find a numerically satisfactory physical frame basis function we rely on the procedure devised by Tesini [17] and described in detail in Bassi, Botti, Colombo, Di Pietro and Tesini [3]. In this latter work, starting from a monomial basis for each elementary space $\mathbb{P}^k(E)$, $E \in \mathcal{T}_h$, an orthonormal basis is inferred by means of the modified Gram-Schmidt orthogonalization procedure. As a result the elementary mass matrices are unit diagonal, independently from the element shapes, and, thanks to the introduction of a suitable element frame, the newly constructed basis provides optimal results from the conservation property viewpoint.

2.2 Reference Frame Basis and Mapping Functions

The definition of basis functions over auxiliary reference frame polygons and the use of reference-to-physical frame mappings are consolidated strategies for the construction of discrete approximation spaces. To introduce mapping functions we first define the reference square $\widehat{E} \stackrel{\text{def}}{=} \{\boldsymbol{\xi} \mid 0 \le \xi_1, \xi_2 \le 1\}$, where ξ_1, ξ_2 are the reference frame Cartesian coordinates, and we let

(i) $\mathbb{Q}^k(\widehat{E})$ be the restriction to $\widehat{E}$ of the polynomial space of tensor-product expansions of two variables and total degree $\le k$ for each variable, so that $N_{\text{dof}}^{\mathbb{Q}^k} = (k+1)^2$.
(ii) $\mathbb{S}^k(\widehat{E})$ be the restriction to $\widehat{E}$ of a serendipity polynomial space of two variables, that is any set containing all the k degree polynomials that can be determined uniquely by the edge nodes, see e.g. Brenner and Scott [5, Sect. 4.6].

We assume that, for all $E \in \mathcal{T}_h$, there exists a polynomial mapping $\Psi_E : \widehat{E} \to E$ such that $\Psi_E \in \mathbb{Q}^m(\widehat{E})$ or $\Psi_E \in \mathbb{S}^m(\widehat{E})$ for some $m \ge 1$ and $E = \Psi_E(\widehat{E})$. In the finite element practice the mapping space as well as the mapping degree m is chosen according to the number of nodes of the physical frame element N_{nodes}^E, so that

$$N_{\text{dof}}^{\mathbb{Q}^m} = N_{\text{nodes}}^E \quad \text{or} \quad N_{\text{dof}}^{\mathbb{S}^m} = N_{\text{nodes}}^E. \tag{3}$$

Accordingly, a mapping Ψ_E of degree m allows to map the reference square $\widehat{E}$ to any non-degenerated quadrilateral element with the prescribed number of nodes. As a matter of fact, we remark that Lagrange polynomials over a set of nodes $N_{\text{nodes}}^{\widehat{E}} = N_{\text{nodes}}^E$ can be obtained solving linear systems involving the generalized Vandermonde matrix associated to $\mathbb{Q}^m(\widehat{E})$ or $\mathbb{S}^m(\widehat{E})$ where m in chosen according to (3), see e.g. Karniadakis and Sherwin [11, Sect. 3.3.2]. For example, in case of arbitrarily shaped, non-degenerated eight- and nine-node quadrilaterals the polynomial spaces $\mathbb{S}^2(\widehat{E})$ and $\mathbb{Q}^2(\widehat{E})$, admitting basis functions $\Phi^2_{\mathbb{S}(\hat{E})} = \{1, \xi_1, \xi_2, \xi_1^2, \xi_1\xi_2, \xi_2^2, \xi_1^2\xi_2, \xi_1\xi_2^2\}$ and $\Phi^2_{\mathbb{Q}(\hat{E})} = \{1, \xi_1, \xi_2, \xi_1^2, \xi_1\xi_2, \xi_2^2, \xi_1^2\xi_2, \xi_1^2\xi_2^2, \xi_1^2\xi_2^2, \xi_1\xi_2^2\}$, are suitable choices, respectively.

We consider the possibility to perform dG discretization based on the following reference frame discrete spaces

$$\text{Choice 1:} \quad V_{\mathbb{P}}^k \stackrel{\text{def}}{=} \left\{ v_h \in L^2(\Omega) \mid v_h = \hat{v}_h(\Psi_E^{-1}(\mathbf{x})),\ \hat{v}_h \in \mathbb{P}^k(\widehat{E}) \right\}, \tag{4a}$$

$$\text{Choice 2:} \quad V_{\mathbb{Q}}^k \stackrel{\text{def}}{=} \left\{ v_h \in L^2(\Omega) \mid v_h = \hat{v}_h(\Psi_E^{-1}(\mathbf{x})),\ \hat{v}_h \in \mathbb{Q}^k(\widehat{E}) \right\}, \tag{4b}$$

where $\forall E \in \mathcal{T}_h$, $\mathbf{x} = \Psi_E(\boldsymbol{\xi})$. Equations (4a) and (4b) involve the following basis functions definitions

$$\text{Choice 1:} \quad \Phi^k_{\mathbb{P}(\widehat{E})} = \{\varphi_i^{\widehat{E}}\}_{i \in D_{\mathbb{P}^k}} \text{ is a basis for } \mathbb{P}^k(\widehat{E}), \tag{5a}$$

$$\text{Choice 2:} \quad \Phi^k_{\mathbb{Q}(\widehat{E})} = \{\varphi_i^{\widehat{E}}\}_{i \in D_{\mathbb{Q}^k}} \text{ is a basis for } \mathbb{Q}^k(\widehat{E}), \tag{5b}$$

respectively. Inside a generic element $E \in \mathcal{T}_h$ the change of variables $\hat{v}_h = v_h(\Psi_E(\boldsymbol{\xi}))$ allows to express physical frame functions v_h as a linear combination of reference frame basis functions supported by the element. Therefore, even if definitions (4a), (4b) are commonly used in literature, we introduce the following alternative definitions which best fit the approximation theory to be developed in Sect. 3

$$V_{\mathbb{P}}^k \stackrel{\text{def}}{=} \left\{ v_h \in L^2(\Omega) \mid \hat{v}_h = v_h(\Psi_E(\boldsymbol{\xi})) \in \mathbb{P}^k(\widehat{E}), \forall E \in \mathcal{T}_h \right\}, \tag{6a}$$

$$V_{\mathbb{Q}}^{k} \stackrel{\text{def}}{=} \left\{ v_h \in L^2(\Omega) \mid \hat{v}_h = v_h(\Psi_E(\boldsymbol{\xi})) \in \mathbb{Q}^k(\widehat{E}), \forall E \in \mathcal{T}_h \right\}. \tag{6b}$$

In this work, in order to compare reference and physical frame basis function with similar properties, we construct hierarchical L^2-orthonormal expansions on the reference square using Legendre polynomials, as described by Karniadakis and Sherwin [11, Sect. 3.2.2]. It is interesting to remark that, if applied to the reference square, the Gram-Schmidt orthogonalization procedure used to define physical frame basis functions allows to recover exactly the orthogonal basis $\Phi^k_{\mathbb{P}(\widehat{E})}$, see [3].

2.2.1 Additional Settings for Reference Frame Discretizations

In this section we introduce additional tools that will prove to be effective when it comes to analyze the approximation properties of reference frame discretizations. While it is well known that the elements shapes have a strong influence on reference frame discretization based on the discrete spaces $V^k_{\mathbb{P},\mathbb{Q}}$, see e.g. [2], in the sequel we will demonstrate that such influence can be predicted analyzing the properties of the mapping functions.

Let us introduce an alternative mapping order which is independent from the number of nodes of the mesh element but takes into account the element shape and the discrete space properties. $\forall E \in \mathcal{T}_h$, we define the effective mapping order $\mathsf{m}_{\mathbb{P}}$ of Ψ_E associated to the polynomial space $\mathbb{P}$ as the minimum positive integer such that

$$\pi^{\mathsf{m}_{\mathbb{P}}}_{\widehat{E}} \Psi_E = \Psi_E, \tag{7}$$

where $\pi^{\mathsf{m}_{\mathbb{P}}}_{\widehat{E}} : L^2(\widehat{E}) \to \mathbb{P}^{\mathsf{m}_{\mathbb{P}}}(\widehat{E})$ is the L^2-orthogonal projection. Similarly, for the polynomial space $\mathbb{Q}$, $\mathsf{m}_{\mathbb{Q}}$ is the minimum positive integer such that

$$\pi^{\mathsf{m}_{\mathbb{Q}}}_{\widehat{E}} \Psi_E = \Psi_E, \tag{8}$$

where $\pi^{\mathsf{m}_{\mathbb{Q}}}_{\widehat{E}} : L^2(\widehat{E}) \to \mathbb{Q}^{\mathsf{m}_{\mathbb{Q}}}(\widehat{E})$. These latter definitions allow to identify the basis function $\Phi^{\mathsf{m}_{\mathbb{P}}}_{\mathbb{P}(\widehat{E})}$, $\Phi^{\mathsf{m}_{\mathbb{Q}}}_{\mathbb{Q}(\widehat{E})}$ being able to exactly represent the mapping function. Since $\mathbb{P}^k \subset \mathbb{Q}^k \subset \mathbb{P}^{2k}$, the following relation holds true

$$1 \leq \mathsf{m}_{\mathbb{Q}} \leq \mathsf{m}_{\mathbb{P}} \leq 2\mathsf{m}_{\mathbb{Q}}. \tag{9}$$

Consider an eight-node quadrilateral element E such that, according to (3), $\Psi_E \in \mathbb{S}^2$. The effective mapping order values are strongly related to the element shape and to the choice of the discrete polynomial space, that is

(i) Rectangular shape. We get $\mathsf{m}_{\mathbb{P}} = \mathsf{m}_{\mathbb{Q}} = 1$. Note that $N^{\mathbb{P}^1}_{\text{dof}} = 3$ since three vertices are sufficient to define the element shape.
(ii) Non-rectangular shape, straight edges. We get $\mathsf{m}_{\mathbb{P}} = 2$ and $\mathsf{m}_{\mathbb{Q}} = 1$.
(iii) Generic quadrilateral with curved edges. We get $\mathsf{m}_{\mathbb{P}} = 3$ and $\mathsf{m}_{\mathbb{Q}} = 2$.

Clearly the effective mapping order might be uneven on general meshes built to approximate complex domains. In such grids, it is a common practice to increase the domain discretization accuracy by means of layers of curved elements adjacent to the domain boundaries while the large majority of mesh elements maintain an affine mapping.

Thanks to the effective mapping order we are now in the position to introduce a new definition of reference frame polynomial spaces that takes into account additional informations regarding the mapping functions, that is

$$W_{\mathbb{P}}^{k} \stackrel{\text{def}}{=} \left\{ v_h \in L^2(\Omega) \mid \hat{v}_h = v_h(\Psi_E(\boldsymbol{\xi})) \in \mathbb{P}^{k\mathsf{m}_{\mathbb{P}}}(\widehat{E}), \forall E \in \mathcal{T}_h \right\}, \tag{10a}$$

$$W_{\mathbb{Q}}^{k} \overset{\text{def}}{=} \left\{ v_h \in L^2(\Omega) \mid \hat{v}_h = v_h(\Psi_E(\boldsymbol{\xi})) \in \mathbb{Q}^{k\mathrm{m}_{\mathbb{Q}}}(\widehat{E}),\ \forall E \in \mathcal{T}_h \right\}. \tag{10b}$$

Since the polynomial degree of a physical frame function $v_h(\mathbf{x})$ raises proportionally to the effective mapping order when transported to the reference frame, we are lead to consider the effective mapping order in the following basis function definitions

$$\Phi_{\mathbb{P}(\widehat{E})}^{k\mathrm{m}_{\mathbb{P}}} = \{\varphi_i^{\widehat{E}}\}_{i \in D_{\mathbb{P}^{k\mathrm{m}_{\mathbb{P}}}}} \text{ is a basis for } \mathbb{P}^{k\mathrm{m}_{\mathbb{P}}}(\widehat{E}), \tag{11a}$$

$$\Phi_{\mathbb{Q}(\widehat{E})}^{k\mathrm{m}_{\mathbb{Q}}} = \{\varphi_i^{\widehat{E}}\}_{i \in D_{\mathbb{Q}^{k\mathrm{m}_{\mathbb{P}}}}} \text{ is a basis for } \mathbb{Q}^{k\mathrm{m}_{\mathbb{Q}}}(\widehat{E}). \tag{11b}$$

As will be demonstrated in Sect. 3.2 the basis function choices (11a), (11b) associated to the discrete spaces (10a), (10b) allows to recover the optimal convergence properties of affine finite elements on general meshes at the expense of an increased number of degrees of freedom.

3 Approximation Properties

In this section we analyze the approximation properties of physical and reference frame discretizations over sequences of h-refined grids and we emphasize how the overall accuracy might be affected by the discrete space choice. The sub-optimality of complete polynomial expansions compared to the tensor-product polynomial expansions, see definitions (5a), and (5b), on general quadrilateral meshes with straight edges has been demonstrated theoretically by Arnold, Boffi and Falk [2]. Here the results will be generalized to higher-order reference-to-physical frame mapping functions demonstrating that the convergence degradation associated to reference frame discretizations is proportional to the effective mapping order. As opposite physical frame discretizations are not influenced by reference-to-physical frame mappings and provide optimal accuracy for the same number of degrees of freedom on general meshes.

We consider a mesh sequence $(\mathcal{T}_h)_{h\in\mathcal{H}}$ where the countable set $\mathcal{H} \overset{\text{def}}{=} \{x \in \mathbb{R} | x > 0\}$ has 0 as unique accumulation point. Each triangulation in the mesh sequence is conforming and regular in the sense of Brenner and Scott [5, Sect. 4.4]. Mesh regularity implies that there exist $\sigma > 0$ such that for all $E \in \mathcal{T}_h$

$$\rho_E^{\max} \geq \sigma h_E \tag{12}$$

where h_E is the element diameter and $\rho_E^{\max}$ is the diameter of the largest ball B_E contained in E such that E is star-shaped with respect to B_E.

Definition 1 (Optimal polynomial interpolation of the L^2 projector) We say that the mesh sequence $(\mathcal{T}_h)_{h\in\mathcal{H}}$ has optimal polynomial approximation properties if for all $h \in \mathcal{H}$, for all $E \in \mathcal{T}_h$, and for all polynomial degree k, the L^2-orthogonal projection operator $\pi_E^k : L^2(E) \to \mathbb{P}^k(E)$ is such that for all $v \in H^{k+1}(E)$, there holds

$$\|v - \pi_E^k v\|_{L^2(E)} \leq C_{\text{app}} h_E^{k+1} |v|_{H^{k+1}(E)} \tag{13}$$

where C_{app} is independent of h and E.

Although more general estimates based on the $H^{m\in\{0,\dots,k\}}$ norm of the interpolation error can be considered we focus on the L^2 norm which is fully capable to underline the different approximation properties associated to physical and reference space discretizations.

The main theoretical results of this section are Theorem 2 and Theorem 4. In Theorem 2 we tackle the approximation properties of physical frame discretizations on general mesh sequences demonstrating the optimality of the polynomial space $\mathbb{P}^k(\mathcal{T}_h)$. Theorem 4 demonstrates that optimal polynomial interpolation properties can be obtained also for reference frame discretizations based on the discrete spaces $W^k_{\mathbb{P},\mathbb{Q}}$ at the expense of an increased number of degrees of freedom. As a matter of fact, while the discrete spaces $V^k_{\mathbb{P},\mathbb{Q}}$ are affected by a convergence degradation proportional to the effective mapping order, see Theorem 3 and Remark 1, the spaces $W^k_{\mathbb{P},\mathbb{Q}}$ entail an increase of the polynomial degree so to overcome such a convergence degradation.

3.1 Approximation Properties of Physical Frame Discretizations

Optimal approximation properties of regular mesh sequences in the context of physical frame dG discretization can be demonstrated quite easily making use of the variant of the Bramble-Hilbert lemma introduced by Brenner and Scott [5, Sect. 4.3].

Lemma 1 (Bramble-Hilbert) *Let B be a ball in E such that E is star-shaped with respect to B and such that its radius $\rho_E > \frac{1}{2}\rho_E^{\max}$. Let $Q^k v$ be the Taylor polynomial of order k of v averaged over B where $v \in H^k(E)$ and $Q^k v \in \mathbb{P}^{k-1}$. Then*

$$|v - Q^k v|_{H^m(E)} \leq C_{k,\gamma_E} h_E^{k-m} |v|_{H^k(E)}, \quad m \in \{0,\dots,k\}, \tag{14}$$

where $\gamma_E \overset{\text{def}}{=} \frac{h_E}{\rho_E^{\max}}$ is the so called chunkiness parameter for E and, from the assumption of mesh regularity, we have $\frac{1}{\gamma_E} \geq \sigma$.

We refer the reader to the book of Brenner and Scott [5, Chaps. 4, 5] for a definition of averaged Taylor polynomials and a proof.

Optimality of physical frame discretizations is proved in the following theorems.

Theorem 1 *Let $E \in \mathcal{T}_h$ be a mesh element of a regular subdivision $\mathcal{T}_h$. Consider an approximation based on the discrete space $\mathbb{P}^k(\mathcal{T}_h)$ and the L^2-orthogonal projection operator $\pi_E^k : L^2(E) \to \mathbb{P}^k(E)$. Then there exist a positive constant C depending on k and the chunkiness parameter γ_E such that, for all $v \in H^{k+1}(E)$,*

$$\|v - \pi_E^k v\|_{L^2(E)} \leq C_{k,\gamma_E} h_E^{k+1} |v|_{H^{k+1}(E)}. \tag{15}$$

Proof Let B be a ball in E such that E is star-shaped with respect to B and such that its radius $\rho_E > \frac{1}{2}\rho_E^{\max}$. Let $Q^{k+1}v$ be the Taylor polynomial of order $k+1$ of v averaged over B. Using the Bramble-Hilbert Lemma and the fact that $Q^{k+1}v \in \mathbb{P}^k(E)$, it is readily inferred that

$$\|v - \pi_E^k v\|_{L^2(E)} = \min_{p\in\mathbb{P}^k(E)} \|v - p\|_{L^2(E)} \tag{16a}$$

$$\leq \|v - Q^{k+1} v\|_{L^2(E)} \tag{16b}$$

$$\leq C_{k,\gamma_E} h_E^{k+1} |v|_{H^{k+1}(E)}. \tag{16c}$$

□

Theorem 2 *Let $(\mathcal{T}_h)_{h\in\mathcal{H}}$ be a regular mesh sequence. Consider an approximation based on the discrete space $\mathbb{P}^k(\mathcal{T}_h)$ and the L^2-orthogonal projection operator $\pi^k_{\mathcal{T}_h} : L^2(\Omega) \to \mathbb{P}^k(\mathcal{T}_h)$. Then there exist a positive constant $C_{k,\sigma}$ depending on k and the mesh regularity parameter σ such that, for all $v \in H^{k+1}(E)$,*

$$\|v - \pi^k_{\mathcal{T}_h} v\|_{L^2(\Omega)} \leq C_{k,\sigma} h^{k+1} |v|_{H^{k+1}(\Omega)}. \tag{17}$$

Proof Observe that

$$\|v - \pi^k_{\mathcal{T}_h} v\|^2_{L^2(\Omega)} = \sum_{E\in\mathcal{T}_h} \|v - \pi^k_E v\|^2_{L^2(E)} \tag{18a}$$

$$\leq \sum_{E\in\mathcal{T}_h} C^2_{k,\gamma_E} h_E^{2(k+1)} |v|^2_{H^{k+1}(E)} \tag{18b}$$

$$\leq C^2_{k,\sigma} h^{2(k+1)} \sum_{E\in\mathcal{T}_h} |v|^2_{H^{k+1}(E)} \tag{18c}$$

$$\leq C^2_{k,\sigma} h^{2(k+1)} |v|^2_{H^{k+1}(\Omega)} \tag{18d}$$

where we used Theorem 1 to infer (18b) and (18c) follows from the mesh regularity assumption since $\frac{1}{\gamma_E} \geq \sigma$. □

3.2 Approximation Properties of Reference Frame Discretizations

It is well know that reference frame discrete polynomial spaces provide optimal approximation properties on regular mesh sequences in case of affine reference-to-physical frame mappings, see e.g. Brenner and Scott [5, Sect. 4.4]. We here derive estimates on the approximation properties of reference frame discretizations when the sole mesh regularity assumption is introduced. Our procedure involves the identification of a suitable physical frame polynomial space, which is a subset of the reference frame polynomial space at hand, and the use theoretical results derived in the previous section to assess the approximation capabilities.

We first derive some discrete embeddings having the goal to establish a relation between physical and reference frame discrete spaces. The following proposition has been inspired by Arnold, Boffi, Falk [2, Theorem 3].

Proposition 1 *Consider a regular subdivision $\mathcal{T}_h$. Let $\mathsf{m}_\mathbb{P}$ and $\mathsf{m}_\mathbb{Q}$ be the effective mapping orders associated to each $E \in \mathcal{T}_h$, see definitions (7) and (8). Consider the reference frame discrete dG spaces $W^k_\mathbb{P}$ and $W^k_\mathbb{Q}$, see definitions (10a), (10b). The following relations holds true*

$$W^k_\mathbb{P} \supseteq \mathbb{P}^k(\mathcal{T}_h) \quad \text{and} \quad W^k_\mathbb{Q} \supseteq \mathbb{P}^k(\mathcal{T}_h). \tag{19}$$

Proof $\forall E \in \mathcal{T}_h$, if $p(\mathbf{x})$ is a polynomial of degree at most k, then

$$p(\Psi_E(\boldsymbol{\xi})) \in \mathbb{P}^k(E) \circ \mathbb{P}^{\mathsf{m}_\mathbb{P}}(\widehat{E}) \subseteq \mathbb{P}^{k\mathsf{m}_\mathbb{P}}(\widehat{E}),$$

and

$$p(\Psi_E(\boldsymbol{\xi})) \in \mathbb{P}^k(E) \circ \mathbb{Q}^{\mathsf{m}_\mathbb{Q}}(\widehat{E}) \subseteq \mathbb{Q}^{k\mathsf{m}_\mathbb{Q}}(\widehat{E}).$$

Therefore $p \in W^k_{\mathbb{P}}$ and $p \in W^k_{\mathbb{Q}}$. □

The approximation properties of reference frame discretizations are tackled in the following theorems.

Theorem 3 *Let $E \in \mathcal{T}_h$ be a mesh element of a regular subdivision $\mathcal{T}_h$ and let $\mathsf{m}_{\mathbb{P}}$, $\mathsf{m}_{\mathbb{Q}}$ be the effective mapping order associated to Ψ_E and the polynomial spaces $\mathbb{P}^k(\widehat{E})$, $\mathbb{Q}^k(\widehat{E})$, respectively, see definitions (7) and (8). Consider the L^2-orthogonal projection operator $\pi^k_{\widehat{E}} : L^2(\widehat{E}) \to \mathbb{P}^k, \mathbb{Q}^k(\widehat{E})$, such that, for all $v \in P^t(E)$*

$$\pi^k_{\widehat{E}}(v \circ \Psi_E) = (\pi^t_E v) \circ (\pi^{\mathsf{m}_{\mathbb{P},\mathbb{Q}}}_{\widehat{E}} \Psi_E) = v \circ \Psi_E, \tag{20}$$

where $t = \lfloor \frac{k}{\mathsf{m}_{\mathbb{P},\mathbb{Q}}} \rfloor$ and $\pi^t_E : L^2(E) \to \mathbb{P}^t(E)$. Then there exist a positive constant C_{t,γ_E} depending on t and the chunkiness parameter γ_E such that, for all $v \in H^{t+1}(E)$,

$$\|v - (\pi^k_{\widehat{E}}(v \circ \Psi_E)) \circ \Psi_E^{-1}\|_{L^2(E)} \leq C_{t,\gamma_E} h_E^{t+1} |v|_{H^{t+1}(E)}. \tag{21}$$

Proof By means of Proposition 1 we are able to infer that $\mathbb{P}^k(\hat{E}) \supseteq \mathbb{P}^{\lfloor \frac{k}{\mathsf{m}_{\mathbb{P}}} \rfloor}(E)$ and $\mathbb{Q}^k(\hat{E}) \supseteq \mathbb{P}^{\lfloor \frac{k}{\mathsf{m}_{\mathbb{Q}}} \rfloor}(E)$. Therefore,

$$\|v - (\pi^k_{\widehat{E}}(v \circ \Psi_E)) \circ \Psi_E^{-1}\|_{L^2(E)} \leq \|v - ((\pi^t_E v) \circ (\pi^{\mathsf{m}_{\mathbb{P},\mathbb{Q}}}_{\widehat{E}} \Psi_E) \circ \Psi_E^{-1})\|_{L^2(E)} \tag{22a}$$

$$= \|v - \pi^t_E v\|_{L^2(E)} \tag{22b}$$

$$\leq C_{t,\gamma_E} h_E^{t+1} |v|_{H^{t+1}(E)}, \tag{22c}$$

where we have used the definition of effective mapping order, that is $\pi^{\mathsf{m}_{\mathbb{P},\mathbb{Q}}}_{\widehat{E}} \Psi_E = \Psi_E$, to obtain (22b) and Theorem 1 in the last step. □

Remark 1 According to Theorem 3 the convergence rate of the L^2-orthogonal projection onto the discrete spaces $\mathbb{P}^k(\widehat{E})$, $\mathbb{Q}^k(\widehat{E})$ is strongly affected by the effective mapping order, which might also be uneven over $\mathcal{T}_h$. In order to investigate the approximation properties of the space $V^k_{\mathbb{P},\mathbb{Q}}$ it is useful to introduce the maximum and the minimum effective mapping order of the triangulation

$$M_{\mathbb{P},\mathbb{Q}} \stackrel{\text{def}}{=} \max_{E \in \mathcal{T}_h} (\mathsf{m}_{\mathbb{P},\mathbb{Q}}) \quad \text{and} \quad \mathcal{M}_{\mathbb{P},\mathbb{Q}} \stackrel{\text{def}}{=} \min_{E \in \mathcal{T}_h} (\mathsf{m}_{\mathbb{P},\mathbb{Q}}). \tag{23}$$

Consider the L^2-orthogonal projection $\pi_{V^k_{\mathbb{P},\mathbb{Q}}} : L^2(\Omega) \to V^k_{\mathbb{P},\mathbb{Q}}$, such that

$$\|v - \pi_{V^k_{\mathbb{P},\mathbb{Q}}} v\|^2_{L^2(\Omega)} = \sum_{E \in \mathcal{T}_h} \|v - (\pi^k_{\widehat{E}}(v \circ \Psi_E)) \circ \Psi_E^{-1}\|^2_{L^2(E)}. \tag{24}$$

Using Theorem 3 and proceeding as in the proof of Theorem 2, for some regular enough function v, the estimated convergence rates are as follows

(i) Uniform effective mapping order over the regular mesh sequence $(\mathcal{T}_h)_{h \in \mathcal{H}}$. Since, for all $h \in \mathcal{H}$, $\max_{E \in \mathcal{T}_h}(\mathsf{m}_{\mathbb{P},\mathbb{Q}}) = \min_{E \in \mathcal{T}_h}(\mathsf{m}_{\mathbb{P},\mathbb{Q}})$, the operator $\pi_{V^k_{\mathbb{P},\mathbb{Q}}}$ is such that

$$\|v - \pi_{V^k_{\mathbb{P},\mathbb{Q}}} v\|_{L^2(\Omega)} = o\Big(h^{\lfloor \frac{k}{M_{\mathbb{P},\mathbb{Q}}} \rfloor + 1}\Big). \tag{25}$$

(ii) Unit asymptotic effective mapping order for the mesh sequence $(\mathcal{T}_h)_{h\in\mathcal{H}}$. Since $M_{\mathbb{P},\mathbb{Q}} \to 1$ as $h \to 0$, the operator $\pi_{V^k_{\mathbb{P},\mathbb{Q}}}$ is such that

$$\|v - \pi_{V^k_{\mathbb{P},\mathbb{Q}}} v\|_{L^2(\Omega)} = o\big(h^{k+1}\big), \tag{26}$$

that is we obtain the convergence rate associated with affine finite elements.

The case of uneven mapping orders over the triangulation would require a specific treatment as the convergence rate varies in each $E \in \mathcal{T}_h$. Nevertheless, it makes sense to conclude that the approximation error in L^2 norm behave as $o(h^c)$, where $\lfloor \frac{k}{M_{\mathbb{P},\mathbb{Q}}} \rfloor + 1 \le c \le \lfloor \frac{k}{\mathcal{M}_{\mathbb{P},\mathbb{Q}}} \rfloor + 1$.

Theorem 4 *Let $(\mathcal{T}_h)_{h\in\mathcal{H}}$ be a regular mesh sequence and let $\mathsf{m}_{\mathbb{P}}$, $\mathsf{m}_{\mathbb{Q}}$ be the effective mapping orders associated to each $E \in \mathcal{T}_h$, see definitions (7) and (8). Consider the discrete space $W^k_{\mathbb{P},\mathbb{Q}}$ and the L^2-orthogonal projection operator $\pi_{W^k_{\mathbb{P},\mathbb{Q}}} : L^2(\Omega) \to W^k_{\mathbb{P},\mathbb{Q}}$ such that, for all $v \in P^k(\mathcal{T}_h)$*

$$\pi_{W^k_{\mathbb{P},\mathbb{Q}}} v = \sum_{E\in\mathcal{T}_h} \pi_{\widehat{E}}^{k\mathsf{m}_{\mathbb{P},\mathbb{Q}}}(v \circ \Psi_E) = \sum_{E\in\mathcal{T}_h} (\pi^k_E v) \circ (\pi_{\widehat{E}}^{\mathsf{m}_{\mathbb{P},\mathbb{Q}}} \Psi_E) = (\pi^k_{\mathcal{T}_h} v) \circ \Psi_E = v \circ \Psi_E. \tag{27}$$

Then there exist a positive constant $C_{k,\sigma}$ depending on k and the mesh regularity parameter σ such that, for all $v \in H^{k+1}(E)$,

$$\|v - \pi_{W^k_{\mathbb{P},\mathbb{Q}}} v\|_{L^2(\Omega)} \le C_{k,\sigma} h^{k+1} |v|_{H^{k+1}(\Omega)}. \tag{28}$$

Proof By means of Proposition 1 we are able to prove that $W^k_{\mathbb{P},\mathbb{Q}} \supseteq \mathbb{P}^k(\mathcal{T}_h)$, so that

$$\|v - \pi_{W^k_{\mathbb{P},\mathbb{Q}}} v\|_{L^2(\Omega)} \le \|v - \pi^k_{\mathcal{T}_h} v\|_{L^2(\Omega)} \tag{29}$$

Thus, using Theorem 2, the result follows. □

Remark 2 According to Theorem 4 the discrete spaces $W^k_{\mathbb{P}}$ and $W^k_{\mathbb{Q}}$ provide optimal polynomial interpolation on regular mesh sequences, see Definition 1. However, since the degree of reference frame polynomial spaces raises proportionally to the effective mapping order in each $E \in \mathcal{T}_h$, see definitions (10a) and (10b), the resulting number of degrees of freedom is suboptimal compared to physical frame discretizations based on the space $\mathbb{P}^k(\mathcal{T}_h)$. Moreover, if the effective mapping order is not uniform over $\mathcal{T}_h$, the degree of reference frame basis functions $\Phi^{k\mathsf{m}_{\mathbb{P}}}_{\mathbb{P}(\widehat{E})}$ and $\Phi^{k\mathsf{m}_{\mathbb{Q}}}_{\mathbb{Q}(\widehat{E})}$ associated to spaces $W^k_{\mathbb{P}}$ and $W^k_{\mathbb{Q}}$, respectively, has to be evaluated on each mesh element.

In this section we considered the approximation properties of reference frame discretization over a sequence of regular h-refined grids, clearly also p-convergence is affected by convergence degradation. In this latter context the drawback is even more evident since the mesh does not change and the effective mapping order is fixed. Both h- and p-convergence will be considered in the following section to numerically assess the approximation properties of physical and reference frame discretizations.

Table 1 Reference-to-physical frame polynomial mapping properties associated to the square, L-shaped and circular mesh families, see Figs. 1 and 2

	Square and L-shaped meshes			Circular meshes		
Quadrilaterals nodes number	4	8	9	4	8	9
Mapping space	$\mathbb{Q}^1$	$\mathbb{S}^2$	$\mathbb{Q}^2$	$\mathbb{Q}^1$	$\mathbb{S}^2$	$\mathbb{Q}^2$
$M_{\mathbb{P}} = \max_{E\in\mathcal{T}_h}(\mathsf{m}_{\mathbb{P}})$	2	3	4	2	3	4
$\mathcal{M}_{\mathbb{P}} = \min_{E\in\mathcal{T}_h}(\mathsf{m}_{\mathbb{P}})$	2	3	4	1	1	1
$M_{\mathbb{Q}} = \max_{E\in\mathcal{T}_h}(\mathsf{m}_{\mathbb{Q}})$	1	2	2	1	2	2
$\mathcal{M}_{\mathbb{Q}} = \min_{E\in\mathcal{T}_h}(\mathsf{m}_{\mathbb{Q}})$	1	2	2	1	1	1
$\lim_{h\to 0}(M_{\mathbb{P}})$	2	3	4	2	2	2
$\lim_{h\to 0}(M_{\mathbb{Q}})$	1	2	2	1	1	1

4 Numerical Test Cases

We consider the following four-, eight- or nine-node quadrilateral elements regular mesh sequences

- uniformly refined mesh family approximating the unit circle $\Omega = \{x^2 + y^2 < 1\}$ hereafter referred to as *circular mesh family* (see Figs. 1(a) and 2(a)),
- uniformly refined randomly distorted mesh family of the square $\Omega = (-1, 1)^2$ hereafter referred to as *square mesh family* (see Figs. 1(b) and 2(b)),
- uniformly refined randomly distorted mesh family of the L-shaped domain $\Omega = (-1, 1)^2 \setminus (0, 1)^2$ hereafter referred to as *L-shaped mesh family* (see Figs. 1(c) and 2(c)).

All the grids here considered have been checked to ensure positivity of the reference-to-physical frame mapping Jacobian in each mesh element. This guarantees that the quadrilaterals do not degenerate in triangular elements and that the edges of each quadrilateral do not intersect each other. Since bilinear elements are less sensitive than biquadratic elements to the occurrence of negative Jacobians, the former have been heavily distorted, compare Fig. 1 with Fig. 2.

The properties of the mesh sequences are summarized in Table 1. The polynomial space of the mapping order, the maximum and minimum effective mapping order of the triangulation, that is $M_{\mathbb{P},\mathbb{Q}} = \max_{E\in\mathcal{T}_h}(\mathsf{m}_{\mathbb{P},\mathbb{Q}})$ and $\mathcal{M}_{\mathbb{P},\mathbb{Q}} = \min_{E\in\mathcal{T}_h}(\mathsf{m}_{\mathbb{P},\mathbb{Q}})$, and the maximum asymptotic effective mapping order, that is $\lim_{h\to 0}(M_{\mathbb{Q}})$, are tabulated to appreciate their influence on convergence results presented hereafter. As expected the higher effective mapping order values are associated to the polynomial space $\mathbb{P}$, as a matter of fact $\mathbb{P}^4 \supset \mathbb{Q}^2$, resulting in $\mathsf{m}_{\mathbb{P}} = 4$ over nine-node mesh sequences, and $\mathbb{P}^3 \supset \mathbb{S}^2$, resulting in $\mathsf{m}_{\mathbb{P}} = 3$ over eight-node mesh sequences. It is interesting to remark that h-refinement on the circular mesh family increases the number of elements along the circumference, thereby leading to quadrilaterals with less and less curved edges, that is $\lim_{h\to 0}(M_{\mathbb{Q}}) = 1$. However, since along the refinement process the internal nodes are treated with some smoothing iterations having the goal to optimize the mesh step size, non-rectangular elements are still present as $h \to 0$, so that $\lim_{h\to 0}(M_{\mathbb{P}}) = 2$. The maximum and minimum value of $\mathsf{m}_{\mathbb{P},\mathbb{Q}}$ over the circular mesh sequence clearly indicates an uneven distribution of the effective mapping order. On the other hand, the distortion acting on square and L-shaped mesh family is self-similar meaning that nodes displacements are proportional the mesh step size, so that $\lim_{h\to 0}(M_{\mathbb{Q}}) = \lim_{h\to 0}(\mathcal{M}_{\mathbb{Q}}) = 2$ and $\lim_{h\to 0}(M_{\mathbb{P}}) = \lim_{h\to 0}(\mathcal{M}_{\mathbb{P}}) = 4$.

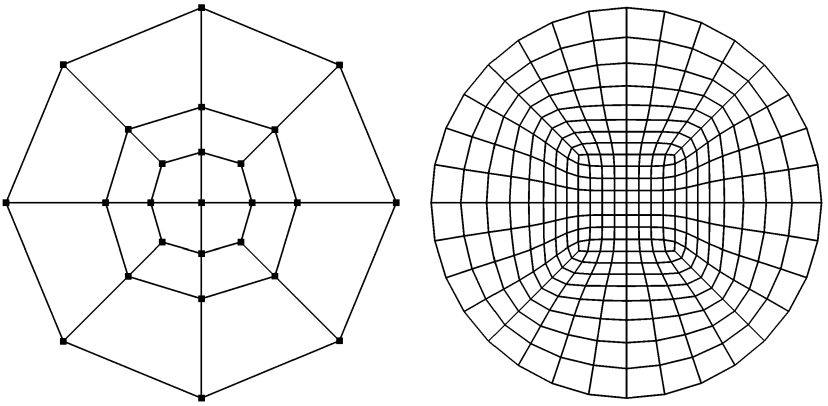

(a) *Circular mesh family. 20 and 320 quadrilateral grids approximating the unit circle.*

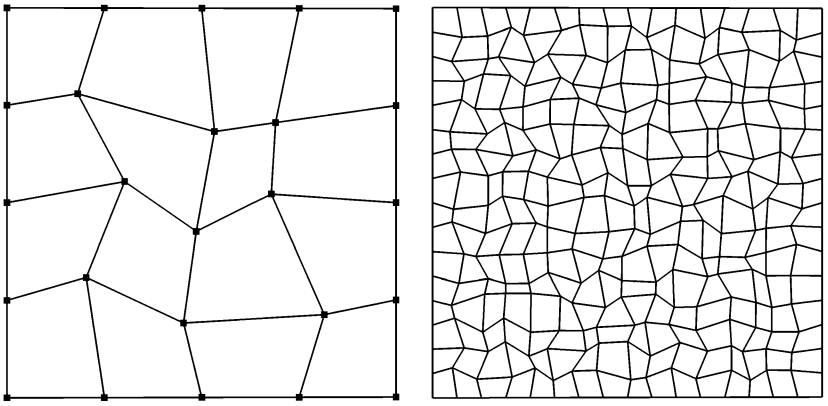

(b) *Randomly distorted square mesh family. 4×4 and 16×16 grids.*

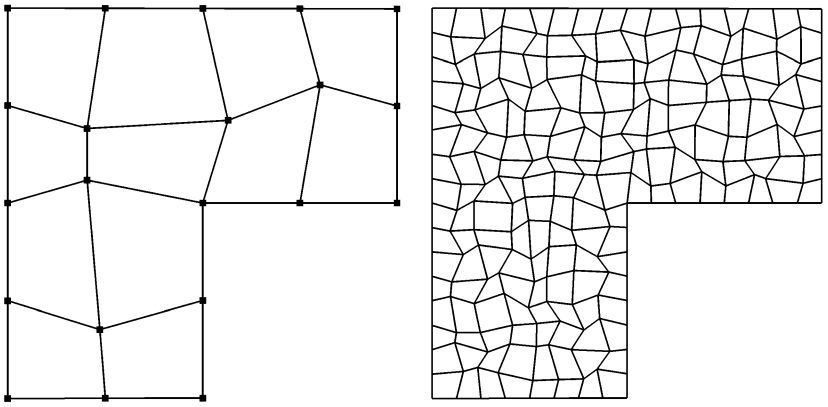

(c) *Randomly distorted L-shaped mesh family. 12 and 192 quadrilateral grids.*

Fig. 1 Four-node circular and square mesh families used to evaluate the h-convergence rate of the L^2-orthogonal projection. Four-node L-shaped mesh family used to evaluate the h-convergence rate of the Interior Penalty discretization of the Laplace equation. Nodes locations are highlighted with *square markers* on the coarsest meshes

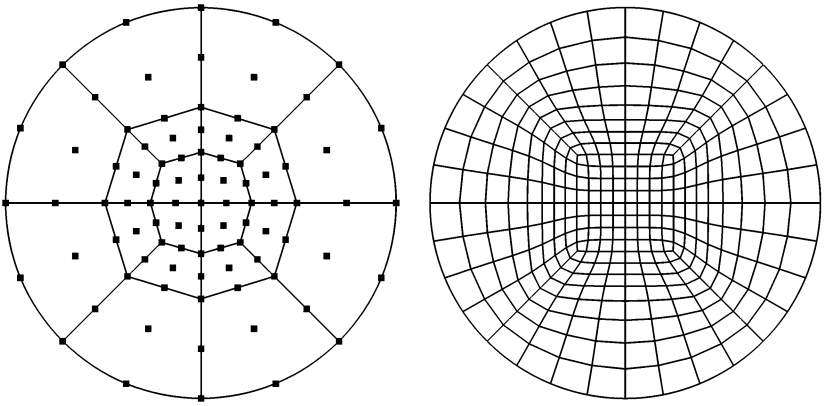

(a) *Circular mesh family. 20 and 320 quadrilateral grids approximating the unit circle.*

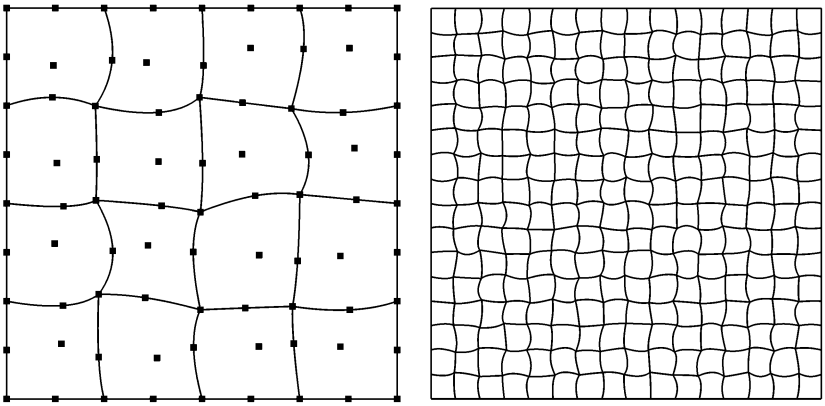

(b) *Randomly distorted square mesh family. 4×4 and 16×16 grids.*

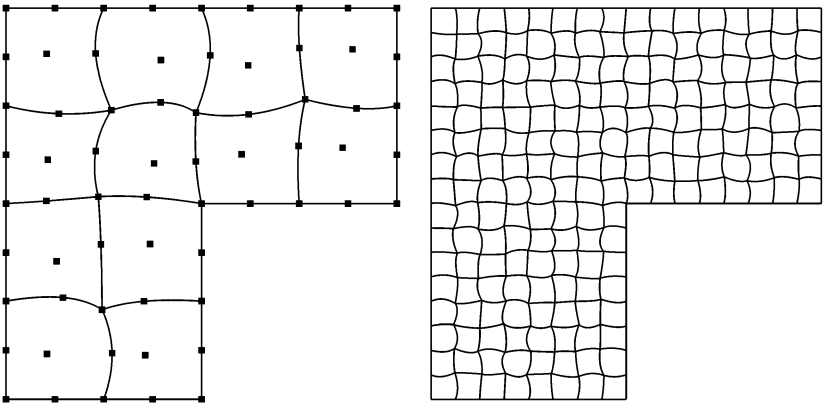

(c) *Randomly distorted L-shaped mesh family. 12 and 192 quadrilateral grids.*

Fig. 2 Eight- and nine-node circular and square mesh families used to evaluate the h-convergence rate of the L^2-orthogonal projection. Eight- and nine-node L-shaped mesh family used to evaluate the h-convergence rate of the Interior Penalty discretization of the Laplace equation. Nodes locations are highlighted with *square markers* on the nine-node coarsest meshes

For the sake of simplicity in all the convergence diagrams presented hereafter we use some abbreviations to indicate the basis function choices, that is

- RF, CP → Reference Frame, Complete Polynomial expansion → the basis function $\Phi^k_{\mathbb{P}(\widehat{E})}$ for the discrete space $V^k_{\mathbb{P}}$,
- RF, TP → Reference Frame, Tensor-Product polynomial expansion → the basis function $\Phi^k_{\mathbb{Q}(\widehat{E})}$ for the discrete space $V^k_{\mathbb{Q}}$,
- PF, CP → Physical Frame, Complete Polynomial expansion → the basis function Φ^k for the discrete space $\mathbb{P}^k(\mathcal{T}_h)$.

4.1 Numerical Integration

In the context of physical frame discretizations numerical integration deserves particular attention. Since Gaussian quadrature formulas are typically available only on reference frame polygons, the integral of a generic physical frame polynomial basis function $\Phi^k_{\mathbb{P}(E)}$ over an element $E \in \mathcal{T}_h$ can be computed as follows:

$$\int_E \Phi^k_{\mathbb{P}(E)}(\mathbf{x})\,\mathrm{d}\mathbf{x} = \int_{\widehat{E}} \Phi^k_{\mathbb{P}(E)}(\Psi_E(\boldsymbol{\xi}))|J_{\Psi_E}(\boldsymbol{\xi})|\,\mathrm{d}\boldsymbol{\xi}, \tag{30}$$

where $\mathbf{x}$ and $\boldsymbol{\xi}$ are physical and reference frame coordinates respectively, and J_{Ψ_E} is the Jacobian of the mapping function Ψ_E. It is clear that the polynomial degree q of the integrand in the last term of (30) results from the product of the polynomial degrees of $\Phi^k_{\mathbb{P}(E)}$, the effective mapping order of Ψ_E ($\mathsf{m}_{\mathbb{P},\mathbb{Q}}$) plus the polynomial degree j of $|J_{\Psi_E}|$ according to the equation

$$q = k\mathsf{m}_{\mathbb{P},\mathbb{Q}} + j. \tag{31}$$

The value of q rapidly increases when considering high order polynomials on curved elements, and so does the number of quadrature nodes required to compute the integral exactly.

It is interesting to remark that in (31) the choice between $\mathsf{m}_{\mathbb{P}}$ and $\mathsf{m}_{\mathbb{Q}}$ is driven by the quadrature formula properties. If the quadrature is designed to integrate tensor-product polynomials, see e.g. Karniadakis and Sherwin [11, Appendix B], $\mathsf{m}_{\mathbb{Q}}$ can be safely employed, as opposite if the quadrature rule exactly integrates polynomials of maximum degree k, see e.g. Stroud [15], $\mathsf{m}_{\mathbb{P}}$ is the correct choice. Alternatively, a physical frame quadrature formula specifically designed for each mesh element could be devised in order to directly integrate the left hand side of (30) and reduce the cost of numerical integration. Such a procedure can be computationally expensive, see e.g. Xiao and Gimbutas [18], but the number of quadrature points could be drastically reduced leading to large savings in time dependent computations.

Consider a nine-nodes quadrilateral element $E \in \mathcal{T}_h$ such that $\mathsf{m}_{\mathbb{Q}} = 2$ and a tensor product quadrature formula on the reference element $\widehat{E}$, it is straightforward to show that reference frame discretizations based on the space $W^k_{\mathbb{Q}}$ and physical frame discretizations based on the space $\mathbb{P}^k(E)$ require exactly the same quadrature order to be exactly integrated on $\widehat{E}$. Note that according to Theorem 4, $\mathbb{P}^k(E)$ and $W^k_{\mathbb{Q}}$ have the same approximation properties over E. Inside E a generic $u_h \in \mathbb{P}^k(\mathcal{T}_h)$ can be expressed as a linear combination of a physical frame basis function $\Phi^k_{\mathbb{P}(E)}$ with coefficients $\mathbf{U}_E \overset{\text{def}}{=} \{U^E_i\}_{i\in D_{\mathbb{P}^k}}$, that is

$$u_h(\mathbf{x})|_E = \sum_{i\in D_{\mathbb{P}^k}} U^E_i \varphi^E_i(\mathbf{x}). \tag{32}$$

Using (30) u_h can be integrated as

$$\int_E u_h(\mathbf{x})\,\mathrm{d}\mathbf{x} = \sum_{i\in D_{\mathbb{P}^k}} \int_E U_i^E \varphi_i^E(\mathbf{x})\,\mathrm{d}\mathbf{x} = \sum_{i\in D_{\mathbb{P}k}} \int_{\widehat{E}} U_i^E \varphi_i^E(\Psi_E(\boldsymbol{\xi}))|J_{\Psi_E}(\boldsymbol{\xi})|\,\mathrm{d}\boldsymbol{\xi}. \tag{33}$$

Since $W_{\mathbb{Q}}^k \supset \mathbb{P}(\mathcal{T}_h)$, inside E u_h can expressed as a linear combination of a reference frame basis function $\Phi_{\mathbb{Q}(\widehat{E})}^{km_{\mathbb{Q}}}$ with coefficients $\mathbf{U}_{\widehat{E}} \overset{\text{def}}{=} \{U_i^{\widehat{E}}\}_{i\in D_{\mathbb{Q}^{km_{\mathbb{Q}}}}}$, that is

$$\hat{u}_h(\boldsymbol{\xi})|_{\widehat{E}} = u_h(\Psi_E(\boldsymbol{\xi}))|_{\widehat{E}} = \sum_{i\in D_{\mathbb{Q}2k}} U_i^{\widehat{E}} \varphi_i^{\widehat{E}}(\boldsymbol{\xi}). \tag{34}$$

The function u_h can be integrated as

$$\int_E u_h(\mathbf{x})\,\mathrm{d}\mathbf{x} = \int_{\widehat{E}} u_h(\Psi_E(\boldsymbol{\xi}))|J_{\Psi_E}(\boldsymbol{\xi})|\,\mathrm{d}\boldsymbol{\xi} = \sum_{i\in D_{\mathbb{Q}2k}} \int_{\widehat{E}} U_i^{\widehat{E}} \varphi_i^{\widehat{E}}(\boldsymbol{\xi})|J_{\Psi_E}(\boldsymbol{\xi})|\,\mathrm{d}\boldsymbol{\xi}. \tag{35}$$

A physical frame basis $\Phi_{\mathbb{P}(E)}^k$ is defined so to span $\mathbb{P}^k(E)$, but the use of a reference frame quadrature formula increases the polynomial order of the integrand according to (31). On the other hand, as stated by Proposition 1, a reference frame basis $\Phi_{\mathbb{Q}(\widehat{E})}^{2k}$ is required to span $\mathbb{P}^k(E)$, therefore demanding the same degree of exactness of $\Phi_{\mathbb{P}(E)}^k$. Clearly, since $\Phi_{\mathbb{P}(E)}^k$ and $\Phi_{\mathbb{Q}(\widehat{E})}^{2k}$ have the same approximation properties over E, the physical frame basis is recommended from the degrees of freedom viewpoint.

As a final note, we remark that physical frame basis function derivatives do not involve the chain rule and can be exactly integrated in the reference frame using the same argument of (30). The required quadrature order can be computed considering that the polynomial order is $k-1$ in place of k in (31).

4.2 L^2-orthogonal Projection Interpolation

We evaluate the approximation properties of the reference and physical frame discrete spaces by means of the L^2-orthogonal projection of

- the sixth degree monomial y^6,
- the sinusoidal function $\sin(x)\sin(y)$.

For all the L^2 projections here considered we employ a tensor-product quadrature rule with a degree of exactness of $2k+1$. We verified that an increased order quadrature rule has no effects on the numerical results both in case of physical and reference frame discretizations. For the evaluation of the error in L^2 norm we increase the quadrature order by a factor four to avoid any bias. From Sect. 4.1 we know that physical frame discretizations would require an higher quadrature order, however, thanks to the orthogonalization procedure involved in physical frame basis definition, see [3], the mass matrix is forced to be unary diagonal yielding optimal results even under inexact integration.

In the next section we consider p-refinement, that is we increase the polynomial degree of the discretization over a fixed mesh, in order to demonstrate the practical implications of Proposition 1, thus, in Sect. 4.2.2, we tackle h-refinement convergence rates.

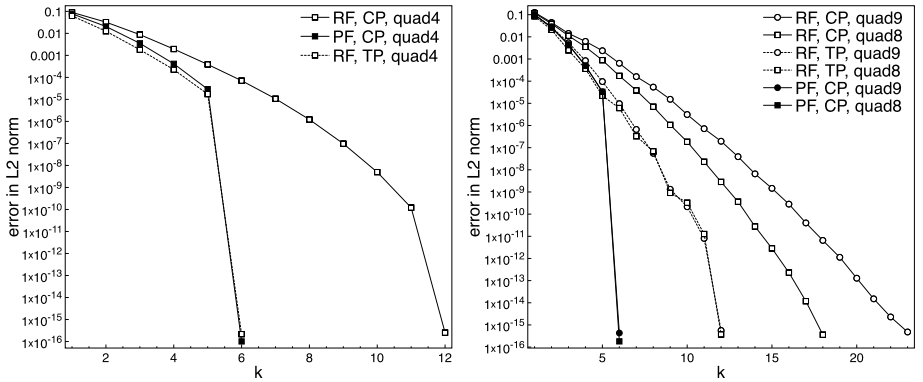

Fig. 3 L^2-orthogonal projection of y^6, p-convergence. *Left*: 20 four-node quadrilateral elements circular mesh, see Fig. 1(a). *Right*: 20 eight- and nine-node quadrilateral elements circular mesh, see Fig. 2(a)

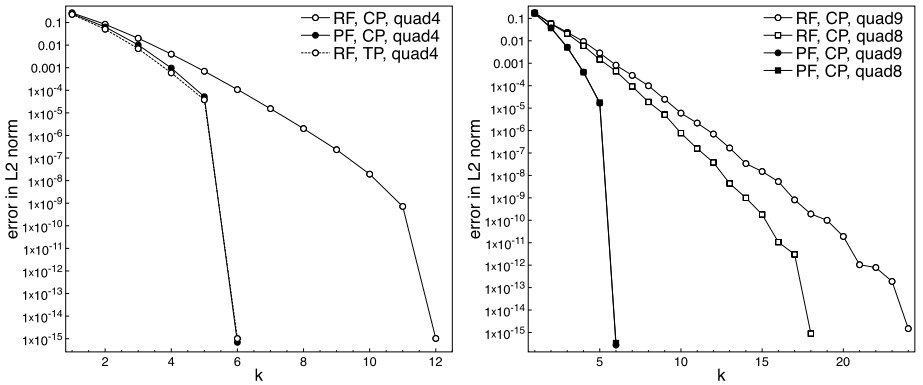

Fig. 4 L^2-orthogonal projection of y^6, p-convergence. *Left*: 4×4 four-node quadrilateral elements distorted square mesh, see Fig. 1(b). *Right*: 4×4 eight- and nine-node distorted square grid, see Fig. 2(b)

4.2.1 Projection of y^6 and $\sin(\pi x)\sin(\pi y)$, p-Refinement

The projection of the sixth order monomial y^6 is useful to understand the impact of the effective mapping order on the properties of a reference frame discrete space. We consider the coarsest meshes of the circular and quadrangular mesh families, see Figs. 1 and 2. The results reported in Figs. 3 and 4 show that a sixth degree physical space basis function Φ^6 yields an L^2-projection of the function y^6 that is exact up to machine precision in the L^2-norm. On the other hand higher-degree reference frame basis functions are often required to accomplish the same task, that is

- $\Phi^6_{\mathbb{Q}(\widehat{E})}$ and $\Phi^{12}_{\mathbb{P}(\widehat{E})}$ for the four-nodes quadrilateral elements mesh,
- $\Phi^{12}_{\mathbb{Q}(\widehat{E})}$ and $\Phi^{18}_{\mathbb{P}(\widehat{E})}$ for an eight-nodes quadrilateral elements mesh,
- $\Phi^{12}_{\mathbb{Q}(\widehat{E})}$ and $\Phi^{24}_{\mathbb{P}(\widehat{E})}$ for a nine-nodes quadrilateral elements mesh,

as predicted by Proposition 1. As a matter of fact, since $W^6_{\mathbb{P},\mathbb{Q}} \supseteq \mathbb{P}^6(\mathcal{T}_h)$, the degree of the reference frame basis able to exactly approximate a sixth order polynomial can be computed

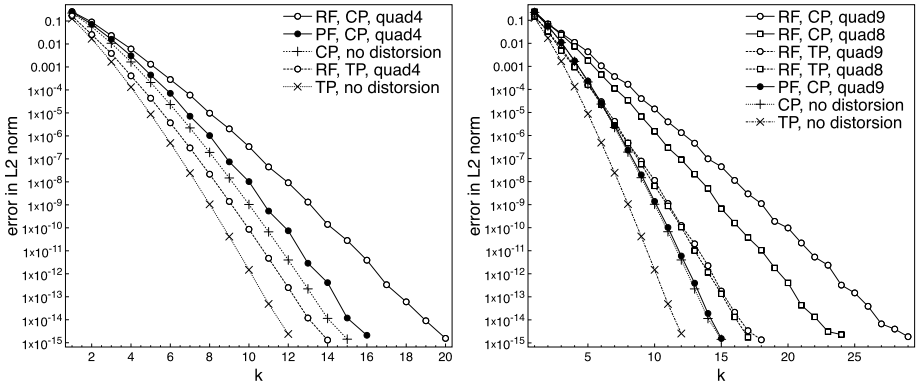

Fig. 5 L^2-orthogonal projection of $\sin(\pi x)\sin(\pi y)$, p-convergence. *Left*: 4×4 four-nodes quadrilateral elements distorted square grid, see Fig. 1(b). *Right*: 4×4 eight- and nine-nodes quadrilateral elements distorted square grid, see Fig. 2(b)

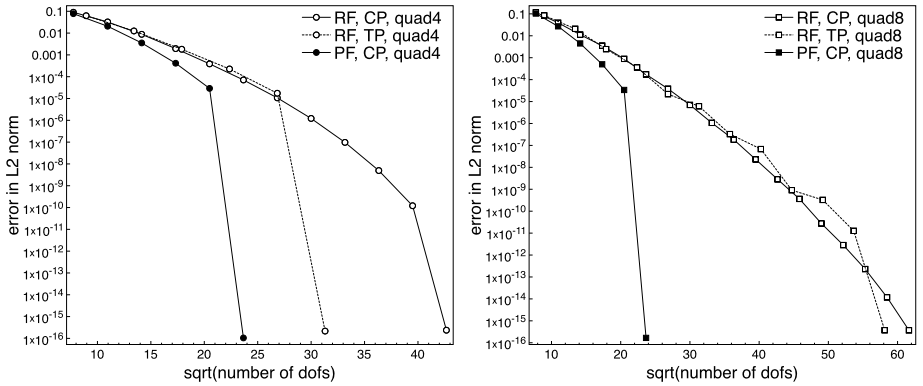

Fig. 6 L^2-orthogonal projection of y^6, p-convergence. *Left*: 20 four-node quadrilateral elements circular mesh, see Fig. 1(a). *Right*: 20 eight- and nine-node quadrilateral elements circular mesh, see Fig. 2(a)

as $k = (6M_{\mathbb{P},\mathbb{Q}})$, using the values of $M_{\mathbb{P},\mathbb{Q}}$ in Table 1. It is interesting to note that the tensor-product basis function $\Phi_{\mathbb{Q}(\widehat{E})}$ has a clear advantage over the basis $\Phi_{\mathbb{P}(\widehat{E})}$ from the required degree viewpoint but this advantage is reduced when the number of degrees of freedom is considered, see Figs. 6 and 7.

We consider the projection of the function $\sin(\pi x)\sin(\pi y)$ over the coarsest mesh of the square mesh family in Fig. 1(b), and compare p-convergence rates with a standard square elements mesh of the computational domain $\Omega = [-1, 1]^2$. Clearly on the square elements grid the basis functions Φ^k and $\Phi^k_{\mathbb{P}(\widehat{E})}$ provide the same results, up to machine precision. The mesh step size h is larger on distorted quadrilateral meshes than on square elements meshes entailing an increase of the L^2 error norm when using physical frame basis functions Φ^k. This aspect is more evident in four-nodes quadrilateral elements meshes than in eight- and nine-nodes quadrilateral elements meshes, see Figs. 5 and 8, because bilinear elements meshes are more distorted. In the interpolation of a non-polynomial function the p-convergence degradation associated to the use of reference frame discrete spaces is more subtle than in the projection of y^6 but it is still present. The advantage of the reference frame

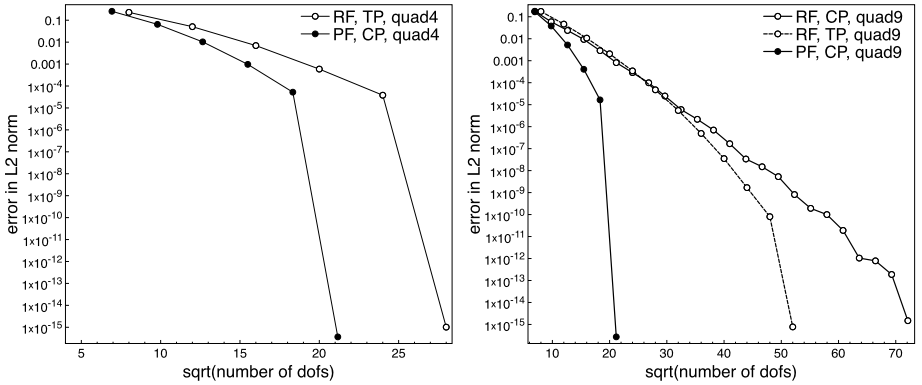

Fig. 7 L^2-orthogonal projection of y^6, p-convergence. *Left*: 4×4 four-node quadrilateral elements distorted square mesh, see Fig. 1(b). *Right*: 4×4 eight- and nine-node distorted square grid, see Fig. 2(b)

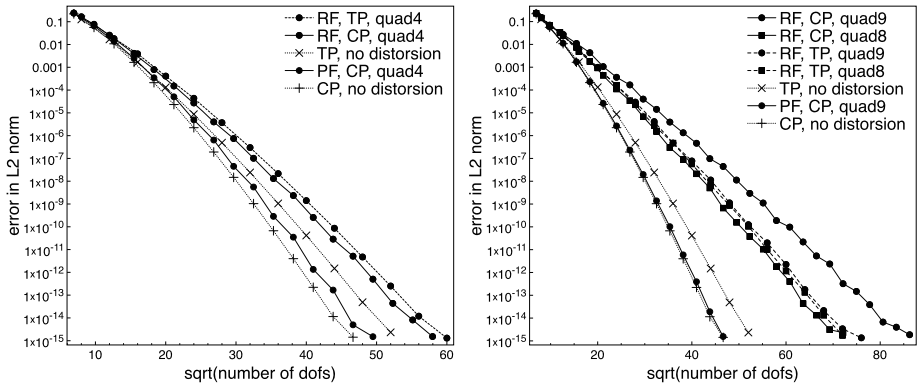

Fig. 8 L^2-orthogonal projection of $\sin(\pi x)\sin(\pi y)$, p-convergence. *Left*: 4×4 four-nodes quadrilateral elements distorted square grid, see Fig. 1(b). *Right*: 4×4 eight- and nine-nodes quadrilateral elements distorted square grid, see Fig. 2(b)

basis $\Phi_{\mathbb{Q}(\widehat{E})}$ over $\Phi_{\mathbb{P}(\widehat{E})}$ is limited to the nine-node quadrilateral elements mesh and, from the degrees of freedom viewpoint, the physical frame basis provides significant gains, see Fig. 8. On the biquadratic quadrilateral elements meshes, the number of degrees of freedom required by the best reference frame discretization to reach machine precision is more than doubled compared to the physical frame discretization.

4.2.2 *Projection of* y^6 *and* $\sin(\pi x)\sin(\pi y)$*, h-Refinement*

h-convergence is assessed over the circular and square mesh families in order to stress the reference-to-physical frame mappings influence on the approximation properties. While in the context of p-refinement the maximum effective mapping order plays the most important role, here also the minimum effective mapping order is of primary importance to predict the convergence rates. Thanks to the theory developed in Sect. 3.2 and using the values of $M_{\mathbb{P},\mathbb{Q}}$ and $\mathcal{M}_{\mathbb{P},\mathbb{Q}}$ reported in Table 1 the theoretical h-convergence rates of reference frame approximations reported within brackets in Tables 2, 3, 4, 5 and 6 easily follow. On the

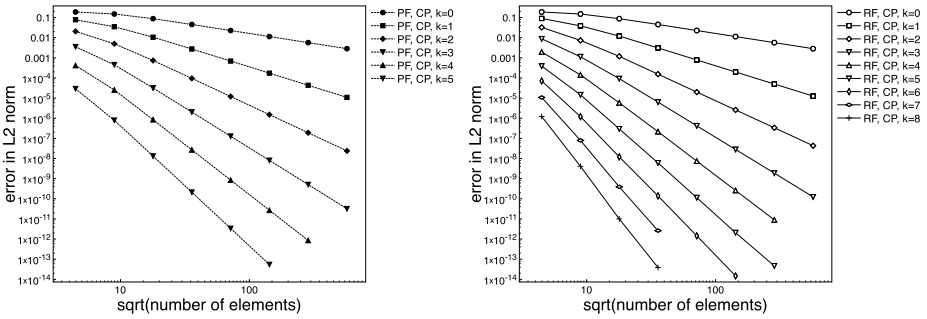

Fig. 9 L^2-orthogonal projection of y^6, h-convergence rates on the four-node quadrilateral elements circular mesh family, see Fig. 1(a)

Table 2 L^2-orthogonal projection of y^6, h-convergence rates for the error in L^2 norm on the four-node quadrilateral elements circular mesh family, see Fig. 1(a). See Fig. 9 for an overview of slopes and error values. The theoretical convergence rate is reported within *brackets*

Projection of y^6, four-node circular mesh family							
n elements	(20) 80	320	1280	5120	20480	81920	327680
	PF, CP						
	convergence rate $(k+1)$						
$k=0$	0.34	0.76	0.95	0.99	0.99	1.0	1.0
$k=1$	1.15	1.72	1.94	1.99	1.99	2.0	2.0
$k=2$	2.04	2.76	2.95	2.98	2.99	2.99	2.99
$k=3$	2.96	3.83	3.96	3.98	3.99	3.99	3.99
$k=4$	4.02	4.91	4.98	4.98	4.98	4.98	
$k=5$	5.21	5.91	5.96	5.98	5.95		
	RF, CP						
	convergence rate (c s.t. $\lfloor k/2 \rfloor + 1 \le c \le k+1$)						
$k=0$	0.34	0.76	0.95	0.99	0.99	1.0	1.0
$k=1$	1.22	1.68	1.95	1.99	1.99	1.99	1.99
$k=2$	2.14	2.63	2.94	2.95	2.94	2.95	2.96
$k=3$	2.96	3.61	3.87	3.91	3.90	3.91	3.93
$k=4$	3.76	4.61	4.76	4.85	4.84	4.85	
$k=5$	4.73	5.62	5.61	5.74	5.77	5.48	
$k=6$	5.88	6.64	6.44	6.59	6.62		
$k=7$	7.08	7.65	7.23				
$k=8$	8.22	8.67	8.02				

other hand k degree physical frame discretizations show h^{k+1} convergence rates in all the configurations here considered.

Over the four-node circular mesh family, even if most of the quadrilateral elements are asymptotically parallelograms, the convergence rates of high-order reference frame discretization based on the space $V_{\mathbb{P}}^k$ are penalized by almost one order because of the maximum effective mapping order ($M_{\mathbb{P}} = 2$), see Fig. 9 and Table 2. Since we address the pro-

jection of y^6 physical frame discretization are considered up to $k = 5$, $k = 6$ would provide machine precision over all the grids of the mesh family. As expected the convergence degradation is more pronounced in the projection of $\sin(\pi x)\sin(\pi y)$ over the distorted square mesh family. Since $M_{\mathbb{P}} = \mathcal{M}_{\mathbb{P}} = 2$ the discrete space $V^k_{\mathbb{Q}}$ provides $h^{\frac{k}{2}+1}$ convergence rates, see Fig. 10 and Table 3.

As predicted by theory, over the nine- and eight-node quadrilateral distorted square mesh family, the L^2-orthogonal projection of y^6 onto the space $V^k_{\mathbb{P}}$ performs as $h^{\lfloor \frac{k}{4} \rfloor + 1}$ and $h^{\lfloor \frac{k}{3} \rfloor + 1}$ respectively, see Table 4. In Fig. 11 it can be readily appreciated that, even if an higher-degree reference frame basis function always provides a better accuracy, a slope increase requires a step of four and three polynomial degrees for nine- and eight-node quadrilaterals grids, respectively. As a result the reference frame basis function $\Phi^{15}_{\mathbb{P}(\widehat{E})}$ provides the same convergence rate of the physical frame basis Φ^3 over the biquadratic distorted square mesh family. The situation improves relying on the basis $\Phi^k_{\mathbb{Q}(\widehat{E})}$, see Fig. 11 and Table 4, but the convergence rate does not exceed $h^{\lfloor \frac{h}{2} \rfloor + 1}$.

The degradation is less dramatic on the biquadratic circular mesh family as $\mathcal{M}_{\mathbb{P}} = 1$ for most of the quadrilaterals elements, implying a lower impact on convergence. Since $\lim_{h \to 0} M_{\mathbb{Q}} = 1$, the basis $\Phi^k_{\mathbb{Q}(\widehat{E})}$ perform as h^{k+1}, in agreement with the affine finite element theory. On the other hand non-rectangular elements penalize the convergence rate of $\Phi^k_{\mathbb{P}(\widehat{E})}$ which behave as h^c, $\lfloor \frac{k}{2} \rfloor + 1 < c < k + 1$, see Fig. 12 and Table 5.

To conclude Fig. 13 and Table 6 allow to appreciate the convergence rates of the $\sin(\pi x)\sin(\pi y)$ L^2-orthogonal projection over the biquadratic square mesh family. As predicted by theory the convergence rate of the best reference frame discretization tops at $h^{\lfloor \frac{k}{2} \rfloor + 1}$ numerically assessing the better performance of physical frame approximations on general meshes.

4.3 L-shaped Domain Laplace Equation Test Case

Here we consider the Interior Penalty (IP) dG discretization of the Poisson equation introduced by Arnold [1] and compare L^2 norm h- and p-convergence rates using physical and reference frame discretizations. We test against the following exact solution of the Laplace equation

$$u = \cos(x)e^y, \tag{36}$$

and impose Dirichlet boundary conditions accordingly.

4.3.1 p-Convergence

As a first point we compare the convergence of physical and reference frame discretization on the coarsest mesh of the L-shaped mesh sequence and also consider the influence of inexact integration on physical frame basis functions. Inexact integration refers to a quadrature rule that allows to exactly integrate a tensor-product polynomial of degree $2k + 1$, while exact integration is approximatively, but safely, imposed considering a tensor-product quadrature formula with a degree of exactness of $4k + 1$, see Sect. 4.1.

Looking at Fig. 14 it is clear that inexact integration affects only the higher polynomial degrees since the stiffness matrix integration error is able to affect the discretization error in these configurations. Moreover, even if under-integrated, the physical frame basis Φ^k provides better accuracy than the reference frame basis $\Phi^k_{\mathbb{P}(\widehat{E})}$, having the same number of

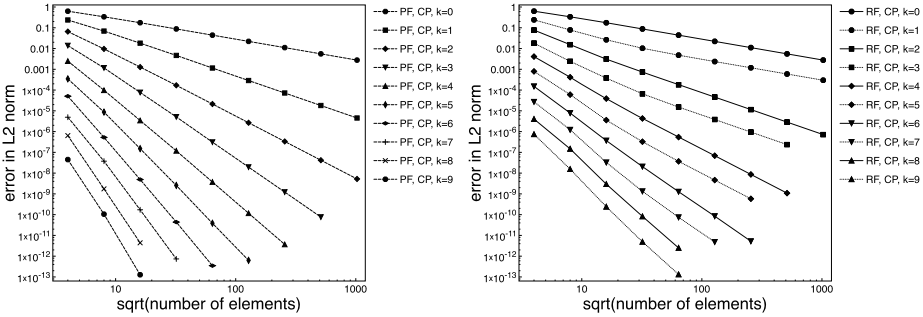

Fig. 10 L^2-orthogonal projection of $\sin(\pi x)\sin(\pi x)$, h-convergence rates on the four-node quadrilateral elements square mesh family, see Fig. 1(b)

Table 3 L^2-orthogonal projection of $\sin(\pi x)\sin(\pi x)$, h-convergence rates for the error in L^2 norm on the four-node quadrilateral elements square mesh family, see Fig. 1(b). See Fig. 10 for an overview of slopes and error values. The theoretical convergence rate is reported within *brackets*

Projection of $\sin(\pi x)\sin(\pi x)$, four-node square mesh family								
n elements	(16) 64	256	1024	4096	16384	65536	262144	1048576
	PF, CP							
	convergence rate $(k+1)$							
$k=0$	0.9	0.95	0.99	0.99	1.0	1.0	1.0	1.0
$k=1$	1.77	1.93	1.96	2.01	2.0	2.0	2.0	2.0
$k=2$	2.77	2.90	2.91	2.99	3.0	3.0	3.0	3.0
$k=3$	3.57	3.92	3.91	4.03	4.0	3.99	4.0	
$k=4$	4.66	4.84	4.85	4.99	5.0	4.99		
$k=5$	5.31	5.84	5.89	6.05	5.94			
$k=6$	6.59	6.74	6.81	6.97				
$k=7$	7.03	7.77	7.86					
$k=8$	8.52	8.62						
$k=9$	8.63	9.69						
	RF, CP							
	convergence rate $(\lfloor k/2 \rfloor + 1)$							
$k=0$	0.9	0.95	0.99	0.99	1.0	1.0	1.0	1.0
$k=1$	1.62	1.57	1.36	1.11	1.02	0.99	1.0	1.0
$k=2$	2.32	2.32	2.05	2.04	1.97	2.0	2.0	2.0
$k=3$	2.90	2.68	2.50	2.12	1.99	2.01	2.0	
$k=4$	3.30	3.42	3.17	2.98	2.97	3.0	3.0	
$k=5$	3.72	4.07	3.45	3.14	3.0	3.0		
$k=6$	4.26	4.40	4.16	4.01	3.91	4.0		
$k=7$	4.47	5.22	4.62	4.15	3.93			
$k=8$	4.76	5.64	5.15	5.04				
$k=9$	5.58	6.01	5.61	5.21				

Table 4 L^2-orthogonal projection of y^6, h-convergence rates for the error in L^2 norm on the eight- and nine-node quadrilateral elements square mesh family, see Fig. 2(b). See Fig. 11 for an overview of slopes and error values. The theoretical convergence rate is reported within *brackets*

Projection of y^6, eight- and nine-node square mesh family								
n elements	(16) 64	256	1024	4096	16384	65536	262144	1048576
	PF, CP, nine-node quadrilaterals							
	convergence rate $(k+1)$							
$k=0$	0.75	0.91	0.97	0.99	0.99	1.0	1.0	1.0
$k=1$	1.71	1.90	1.97	1.99	1.99	2.0	2.0	2.0
$k=2$	2.78	2.91	2.97	2.99	2.98	3.0	3.0	3.0
$k=3$	3.88	3.93	3.97	3.98	3.98	4.0	4.0	
$k=4$	4.96	4.96	4.95	4.98	4.98	4.86		
$k=5$	6.04	6.03	5.94	5.99				
	RF, CP, nine-node quadrilaterals							
	convergence rate $(\lfloor k/4 \rfloor + 1)$							
$k=0$	0.75	0.91	0.97	0.99	0.99	1.0	1.0	1.0
$k=1$	1.71	1.60	1.12	1.08	1.0	1.0	0.99	1.0
$k=2$	1.88	0.89	0.89	0.95	0.96	0.98	0.98	1.0
$k=3$	1.16	0.91	0.85	0.97	1.0	1.0	0.99	
$k=4$	1.58	1.87	1.87	1.97	2.0	2.0	2.0	
$k=5$	2.57	2.65	1.94	2.02	1.98	2.0		
$k=6$	2.42	1.94	1.85	2.0	1.94	2.0		
$k=7$	1.92	1.79	1.85	1.92	2.03	2.01		
$k=8$	2.05	2.98	2.86	2.95	3.02			
$k=9$	3.17	3.62	2.88	3.03	2.95			
$k=10$	2.56	3.12	2.82	3.03	2.97			
$k=11$	2.26	2.76	2.89	2.85	3.09			
$k=12$	2.39	4.09	3.87	3.91				
$k=13$	3.70	4.5	3.78	4.05				
$k=14$	2.65	4.25	3.79	4.04				
$k=15$	2.36	3.84	3.88	3.73				
	RF, CP, eight-node quadrilaterals							
	convergence rate $(\lfloor k/3 \rfloor + 1)$							
$k=0$	0.75	0.91	0.97	0.99	0.99	1.0	1.0	1.0
$k=1$	1.58	1.53	1.21	1.0	0.97	0.99	1.0	0.99
$k=2$	1.42	0.90	0.78	0.87	0.98	0.94	1.0	1.0
$k=3$	1.68	1.81	1.78	1.88	2.0	1.96	2.0	
$k=4$	2.46	2.67	1.95	1.93	2.01	1.95	2.0	
$k=5$	2.26	1.91	1.60	1.84	1.95	1.91		
$k=6$	2.31	2.74	2.65	2.85	2.98	2.93		
$k=7$	2.87	3.71	2.81	2.89	3.02	2.92		
$k=8$	2.32	2.85	2.66	2.85	2.93			
$k=9$	2.63	3.65	3.73	3.84	3.97			
$k=10$	3.30	4.68	3.75	3.85	3.44			
$k=11$	2.33	3.65	3.89	3.82				

Table 4 (*Continued*)

Projection of y^6, eight- and nine-node square mesh family								
n elements	(16) 64	256	1024	4096	16384	65536	262144	1048576
	RF, TP, nine-node quadrilaterals							
	convergence rate ($\lfloor k/2 \rfloor + 1$)							
$k=0$	0.75	0.91	0.97	0.99	0.99	1.0	1.0	1.0
$k=1$	1.72	1.64	1.15	1.09	1.01	0.99	0.99	1.0
$k=2$	2.55	2.13	1.87	2.03	1.93	1.99	2.0	
$k=3$	3.25	2.67	2.11	2.07	2.0	1.98	1.98	
$k=4$	4.01	3.04	2.8	3.01	2.90	2.97		
$k=5$	4.40	3.62	3.05	3.02	2.99	2.97		
$k=6$	5.04	3.98	3.71	3.98	3.9			
$k=7$	5.22	4.65	3.92	3.98	3.91			
$k=8$	5.56	5.04	4.64	4.89				
$k=9$	5.67	5.52	4.82					

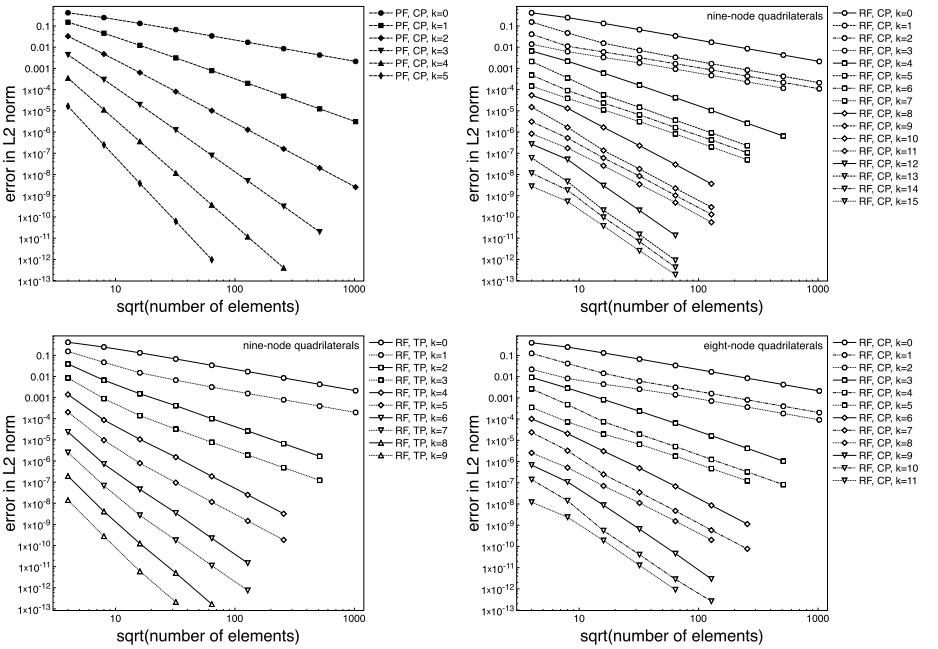

Fig. 11 L^2-orthogonal projection of y^6, h-convergence rates on the eight- and nine-node quadrilateral elements square mesh family, see Fig. 2(b)

degrees of freedom. Since the evaluation of the convergence rates of under-integrated discretizations is not the primary goal of this manuscript, in the following we consider exactly integrated physical frame discretizations. This means that, for the same basis degree, the degree of exactness used for physical frame formulations is almost doubled compared to the $2k+1$ imposed for reference frame discretizations. Since we verified that an increased order

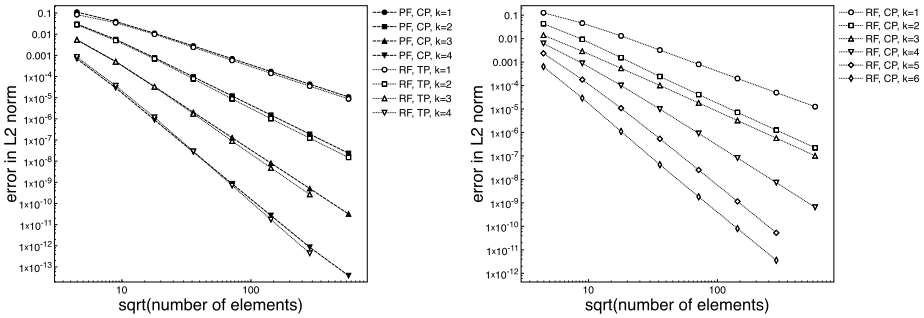

Fig. 12 L^2-orthogonal projection of y^6, h-convergence rates on the nine-node quadrilateral elements circular mesh family, see Fig. 2(a)

Table 5 L^2-orthogonal projection of y^6, h-convergence rates for the error in L^2 norm on the nine-node quadrilateral elements circular mesh family, see Fig. 2(a). See Fig. 12 for an overview of slopes and error values. The theoretical convergence rate is reported within *brackets*

Projection of y^6, nine-node circular mesh family							
n elements	(20) 80	320	1280	5120	20480	81920	327680
	PF, CP						
	convergence rate $(k+1)$						
$k=1$	1.48	1.85	1.99	2.0	2.0	2.0	2.0
$k=2$	2.41	2.88	3.0	3.0	3.0	3.0	3.0
$k=3$	3.40	3.95	4.01	4.0	3.99	3.99	3.99
$k=4$	4.55	5.04	5.03	5.0	4.98	4.99	
	RF, TP						
	convergence rate $(k+1)$						
$k=1$	1.27	1.80	2.04	2.05	2.03	2.01	2.01
$k=2$	2.47	2.87	3.14	3.15	3.1	3.05	3.03
$k=3$	3.44	3.92	4.24	4.27	4.22	4.15	
$k=4$	4.51	4.98	5.32	5.37	5.34	5.28	
	RF, CP						
	convergence rate (c s.t. $\lfloor k/2 \rfloor + 1 \leq c \leq k+1$)						
$k=1$	1.47	1.80	2.0	2.02	2.0	1.99	1.99
$k=2$	2.20	2.59	2.66	2.56	2.51	2.51	2.50
$k=3$	2.27	2.41	2.42	2.47	2.49	2.50	2.50
$k=4$	2.81	3.13	3.34	3.44	3.47	3.49	3.49
$k=5$	3.72	4.03	4.33	4.41	4.44	4.45	
$k=6$	4.45	4.72	4.70	4.54	4.49	4.49	

quadrature formula does not improve the accuracy provided by reference frame discretizations, we are able to conclude that the discretization error dominates the integration error that might arise because of rational reference frame basis function derivatives.

The p-convergence results on the coarsest grids of the L-shaped mesh families confirm the trend observed in the L^2-orthogonal projection, see Figs. 15 and 16. The reference frame

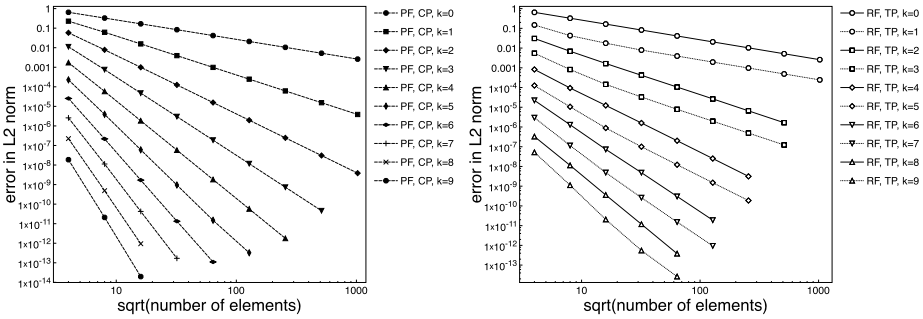

Fig. 13 L^2-orthogonal projection of $\sin(\pi x)\sin(\pi x)$, h-convergence rates on the nine-node quadrilateral elements square mesh family, see Fig. 2(b)

Table 6 L^2-orthogonal projection of $\sin(\pi x)\sin(\pi x)$, h-convergence rates for the error in L^2 norm on the nine-node quadrilateral elements square mesh family, see Fig. 2(b). See Fig. 13 for an overview of slopes and error values. The theoretical convergence rate is reported within *brackets*

Projection of $\sin(\pi x)\sin(\pi x)$, nine-node square mesh family								
n elements	(16) 64	256	1024	4096	16384	65536	262144	1048576
	PF, CP							
	convergence rate $(k+1)$							
$k=0$	0.99	1.0	1.0	1.0	1.0	1.0	1.0	1.0
$k=1$	1.88	1.98	1.99	2.0	2.0	2.0	2.0	2.0
$k=2$	2.89	2.97	3.0	3.0	3.0	3.0	3.0	3.0
$k=3$	3.89	4.0	4.0	4.0	4.0	4.0	4.0	
$k=4$	4.88	5.0	5.0	5.0	5.0	5.0		
$k=5$	5.86	6.02	5.98	6.0	5.51			
$k=6$	6.87	7.0	6.99	6.93				
$k=7$	7.83	8.06	7.97					
$k=8$	8.84	9.01						
$k=9$	9.80	10.05						
	RF, TP							
	convergence rate $(\lfloor k/2 \rfloor + 1)$							
$k=0$	0.99	1.0	1.0	1.0	1.0	1.0	1.0	1.0
$k=1$	1.78	1.28	1.16	1.0	1.01	1.0	1.0	1.0
$k=2$	2.15	2.08	1.93	2.01	2.0	2.0	2.0	
$k=3$	2.74	2.49	2.13	2.07	2.0	2.0	2.0	
$k=4$	3.12	2.92	2.96	2.98	3.0	3.0		
$k=5$	3.57	3.57	3.15	3.03	3.02	3.0		
$k=6$	4.11	4.14	3.92	4.0	4.0			
$k=7$	4.68	4.55	4.23	4.09	4.01			
$k=8$	4.85	4.99	4.91	4.96				
$k=9$	5.53	5.76	5.22	4.38				

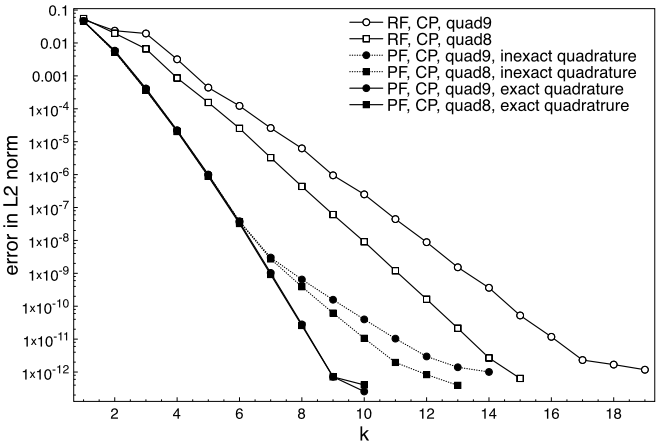

Fig. 14 IP dG discretization of the Laplace equation, p-refinement. 12 eight- and nine-node quadrilateral elements mesh, see Fig. 2(c)

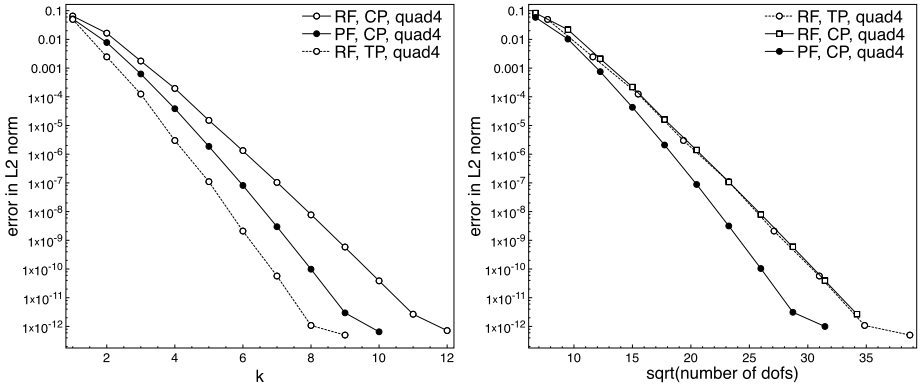

Fig. 15 IP dG discretization of the Laplace equation, p-refinement. 12 four-node quadrilateral elements mesh, see Fig. 1(c)

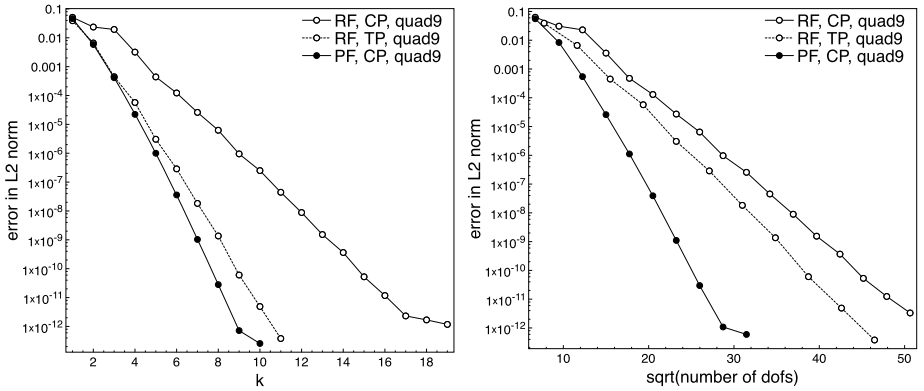

Fig. 16 IP dG discretization of the Laplace equation, p-refinement. 12 nine-node quadrilateral elements mesh, see Fig. 2(c)

Table 7 IP dG discretization of the Laplace equation, h-convergence rates for the error in L^2 norm on the four-node quadrilateral elements L-shaped mesh family, see Fig. 1(c). See Fig. 17 for an overview of slopes and error values. The theoretical convergence rate is reported within *brackets*

Laplace equation, four-node L-shaped mesh family						
n elements	(12) 48	192	768	3072	12288	49152
	PF, CP					
	convergence rate $(k+1)$					
$k=1$	1.44	1.78	1.84	1.98	1.96	2.0
$k=2$	2.77	2.82	3.0	2.97	3.0	3.0
$k=3$	4.05	3.88	3.93	3.99	3.98	
$k=4$	4.92	4.94	4.96	4.99		
	RF, TP					
	convergence rate $(\lfloor k/2 \rfloor + 1)$					
$k=1$	1.25	0.94	0.85	0.79	1.0	0.94
$k=2$	1.73	1.93	1.98	2.0	1.97	2.0
$k=3$	2.07	2.24	2.11	1.88	2.0	
$k=4$	2.64	2.85	2.85	2.93	2.97	
$k=5$	2.40	3.54	2.96	2.83		
$k=6$	3.04	3.70	3.82	3.92		
$k=7$	2.97	4.55	3.62			

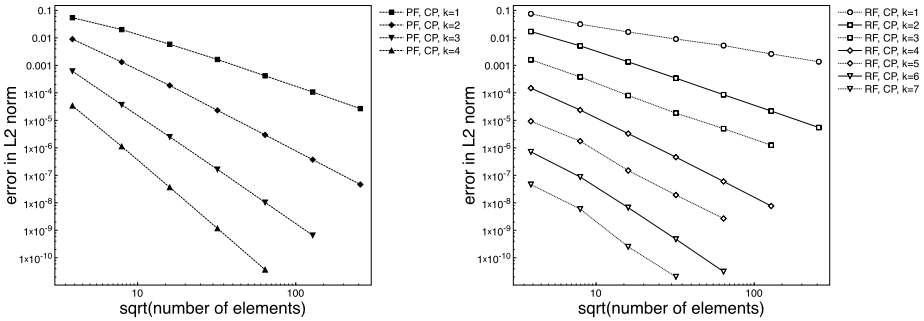

Fig. 17 IP dG discretization of the Laplace equation, h-refinement. Four-node quadrilateral elements L-shaped mesh family, see Fig. 1(c)

basis function $\Phi^k_{\mathbb{Q}(\widehat{E})}$ does not yield a significant advantage over the basis $\Phi^k_{\mathbb{P}(\widehat{E})}$ in terms of degrees of freedom, resulting similarly affected by mesh distortion. From the degrees of freedom viewpoint the accuracy associated to physical frame discretization is unmatchable on general meshes. The price to pay is related to the computational cost of the orthogonalization procedure to be performed on each mesh element and to the increased order quadrature rules required for exact numerical integration.

4.3.2 h-Convergence

Theoretical results regarding the approximation properties of reference and physical frame polynomial spaces are confirmed by h-convergence rates of the IP dG discretization. On the four-node quadrilateral elements L-shaped mesh family ($\mathcal{M}_{\mathbb{P}} = M_{\mathbb{P}} = 2$, see Table 1) the reference frame tensor-product expansion $\Phi^k_{\mathbb{P}(\widehat{E})}$ yields $h^{\lfloor \frac{k}{2} \rfloor + 1}$ convergence rates, see Fig. 17 and Table 7. On the nine-node quadrilateral elements L-shaped mesh family ($\mathcal{M}_{\mathbb{Q}} =$

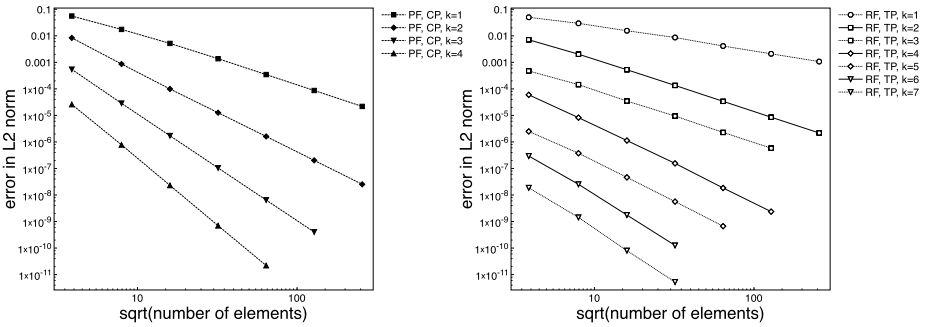

Fig. 18 IP dG discretization of the Laplace equation, h-refinement. Nine-node quadrilateral elements L-shaped mesh family, see Fig. 2(c)

Table 8 IP dG discretization of the Laplace equation, h-convergence rates for the error in L^2 norm on the nine-node quadrilateral elements L-shaped mesh family, see Fig. 2(c). See Fig. 18 for an overview of slopes and error values. The theoretical convergence rate is reported within *brackets*

Laplace equation, nine-node L-shaped mesh family						
n elements	(12) 48	192	768	3072	12288	49152
	PF, CP					
	convergence rate $(k+1)$					
$k=1$	1.67	1.75	1.91	1.99	2.0	2.0
$k=2$	3.26	3.12	2.97	2.97	3.0	3.0
$k=3$	4.24	4.06	4.03	4.01	4.0	
$k=4$	5.06	5.08	5.04	4.99		
	RF, TP					
	convergence rate $(\lfloor k/2 \rfloor + 1)$					
$k=1$	0.75	0.92	0.85	1.07	0.98	0.97
$k=2$	1.80	1.95	1.96	2.0	1.99	1.97
$k=3$	1.71	2.05	1.87	2.05	1.97	
$k=4$	2.85	2.87	2.86	3.08	2.96	
$k=5$	2.63	3.0	3.01			
$k=6$	3.53	3.85	3.80			
$k=7$	3.70	4.15	3.93			

$M_{\mathbb{Q}} = 2$, see Table 1) the reference frame tensor-product expansion $\Phi^k_{\mathbb{Q}(\widehat{E})}$ yields $h^{\lfloor \frac{k}{2} \rfloor + 1}$ convergence rates, see Table 8. Figures 17 and 18 allow to appreciate that a slope increase requires a step of two reference frame basis functions degrees. As a result, a physical frame basis function Φ^3 has the same convergence rate of the reference frame basis $\Phi^6_{\mathbb{Q}(\widehat{E})}$ and $\Phi^7_{\mathbb{Q}(\widehat{E})}$. Once more the convergence rates associated to physical frame discretizations are not impaired by mesh distortion.

5 Conclusion

We estimated the approximation properties of physical and reference frame discontinuous polynomial spaces considering regular mesh sequences and arbitrary order reference-to-physical frame mappings. While physical frame discretizations are not influenced by mapping functions and provide optimal approximation properties on regular meshes, reference

frame discretization might suffer from a degradation of h-convergence on general meshes with distorted or curved elements. The convergence deterioration, which depends on the element shape, the mapping function and the reference frame polynomial space, can be evaluated thanks to the theory here developed. Moreover, analyzing the degree of the reference frame polynomial space which is able to exactly represent the mapping function (here referred as *effective mapping order*), optimal convergence rates can be recovered. This comes at a price since the degree of the reference frame polynomial spaces must be raised proportionally to the effective mapping order.

In the context of non-affine mappings the number of degrees of freedom required to obtain a given accuracy is smaller when physical frame discretizations are employed. These latter might be preferred to reference frame discretizations when h-refinement is not able to drive a mesh sequence towards affine geometric transformations.

References

1. Arnold, D.N.: An interior penalty finite element method with discontinuous elements. SIAM J. Numer. Anal. **19**, 742–760 (1982)
2. Arnold, D.N., Boffi, D., Falk, R.S.: Approximation by quadrilateral finite elements. Math. Comput. **71**(239), 909–922 (2002)
3. Bassi, F., Botti, L., Colombo, A., Di Pietro, D.A., Tesini, P.: On the flexibility of agglomeration based physical space discontinuous Galerkin discretizations. J. Comput. Phys. (2011). doi:10.1016/j.jcp.2011.08.018
4. Bassi, F., Crivellini, A., Di Pietro, D.A., Rebay, S.: An artificial compressibility flux for the discontinuous Galerkin solution of the incompressible Navier-Stokes equations. J. Comput. Phys. **218**, 794–815 (2006)
5. Brenner, S.C., Scott, L.R.: The Mathematical Theory of Finite Element Methods, 3rd edn. Springer, New York (2008)
6. Ciarlet, P.G., Raviart, P.-A.: Interpolation theory over curved elements with applications to finite element methods. Comput. Methods Appl. Mech. Eng. **1**, 217–249 (1972)
7. Di Pietro, D.A., Ern, A.: Mathematical Aspects of Discontinuous Galerkin Methods. Maths & Applications, vol. 69. Springer, Berlin (2011)
8. Ern, A., Guermond, J.-L.: Eléments finís: théorie, applications, mise en œuvre. Mathématiques & Applications, vol. 36. Springer, Berlin (2002)
9. Gassner, G.J., Lörcher, F., Munz, C.-D., Hesthaven, J.S.: Polymorphic nodal elements and their application in discontinuous Galerkin methods. J. Comput. Phys. **228**, 1573–1590 (2009)
10. Georgoulis, E.H.: *hp*-version interior penalty discontinuous Galerkin finite element methods on anisotropic meshes. Int. J. Numer. Anal. Model. **3**, 52–79 (2006)
11. Karniadakis, G.E., Sherwin, S.: Spectral/*hp* Element Methods for Computational Fluid Dynamics. Numerical Mathematics and Scientific Computation. Oxford University Press, Oxford (2005)
12. Kikuchi, F., Okabe, M., Fujio, H.: Modification of the 8-node serendipity element. Comput. Methods Appl. Mech. Eng. **179**, 91–109 (1999)
13. Kurtz, J., Xenophontos, C.: On the effects of using curved elements in the approximation of the Reissner–Mindlin plate by the *p* version of the finite element method. Appl. Numer. Math. **46**, 231–246 (2003)
14. McNeal, R.H., Harder, R.L.: Eight nodes or nine? Int. J. Numer. Methods Eng. **33**, 1049–1058 (1992)
15. Stroud, A.H.: Approximate Calculation of Multiple Integrals. Prentice-Hall, Englewood Cliffs (1971)
16. Suri, M.: Analytical and computational assessment of locking in the *hp* finite element method. Comput. Methods Appl. Mech. Eng. **133**, 347–371 (1996)
17. Tesini, P.: An *h*-multigrid approach for high-order discontinuous Galerkin methods. Ph.D. thesis, Università degli Studi di Bergamo, January 2008
18. Xiao, H., Gimbutas, Z.: A numerical algorithm for the construction of efficient quadrature rules in two and higher dimensions. Comput. Math. Appl. **59**, 663–676 (2010)
19. Zhang, J., Kikuchi, F.: Interpolation error estimates of a modified 8-node serendipity finite element. Numer. Math. **85**, 503–524 (2000)